TITLE

An important role for triglyceride in regulating spermatogenesis

AUTHORS

Charlotte F. Chao[1&], Yanina-Yasmin Pesch[1&], Huaxu Yu[2], Chenjingyi Wang[2], Maria Aristizabal[3], Tao Huan[2], Guy Tanentzapf[1], Elizabeth J. Rideout[1*]

AFFILIATIONS

[1] Department of Cellular and Physiological Sciences, Life Sciences Institute, The University of British Columbia, Vancouver, BC, Canada V6T 1Z3

[2] Department of Chemistry, The University of British Columbia, Vancouver, BC, Canada V6T 1Z1

[3] Department of Biology, Queen's University, Kingston, ON, Canada K7L 3N6

* Corresponding author

[&] Equally contributing authors

[*] Correspondence: elizabeth.rideout@ubc.ca

SUMMARY

Drosophila is a powerful model to study how lipids affect sperm development[1–3]. Studies in flies showed that phosphatidylinositol and its phosphorylated derivatives influence spermatogenesis[4–14], and uncovered roles for membrane lipids and fatty acids in this process[15–19]. Less is known about how neutral lipids, another major lipid group, affect sperm development. Neutral lipids include triglycerides and cholesterol esters, and reside within specialized organelles called lipid droplets (LD)[20]. Emerging evidence shows testis LD are present in normal and stressful contexts[21–26]. Genes associated with neutral lipid metabolism and LD also show testis expression[27–29], and dysregulation of these genes causes subfertility[30–32]. Yet, many questions remain about the spatial, temporal, and cell type-specific requirements for neutral lipids and LD during spermatogenesis. Here, we show that LD are present in early-stage somatic and germline cells within the *Drosophila* testis. We identified a role for triglyceride lipase *brummer* (*bmm*) in regulating testis LD, and show that whole-body and cell-autonomous loss of *bmm* leads to defects in sperm development. Because lipidomic analysis of *bmm* mutants revealed excess triglyceride accumulation, and spermatogenic defects in *bmm* mutants were rescued by genetically blocking triglyceride synthesis, our data suggest that *bmm*-mediated regulation of triglyceride influences sperm development. This identifies triglyceride as an important neutral lipid that contributes to *Drosophila* sperm development, and reveals a key role for *bmm* in regulating testis triglyceride levels and spermatogenesis.

KEYWORDS

Triglyceride, lipid droplet, spermatogenesis, testis, *brummer*, adipose triglyceride lipase (ATGL), lipidomics.

RESULTS AND DISCUSSION

Lipid droplets are present in early-stage somatic and germline cells

We previously reported the presence of small circular punctae (<1 μm) corresponding to LD near the apical tip of the testis[21]. We confirm these results in *w*^{1118} males using neutral lipid stain BODIPY (4,4-Difluoro-1,3,5,7,8-Pentamethyl-4-Bora-3a,4a-Diaza-*s*-Indacene) (Figure 1A,S1A). Importantly, we reproduced this spatial distribution of LD in two independent genetic backgrounds and at two additional ages (Figure 1B,1C). In all cases, LD were in a testis region that contains stem cells and early-stage somatic and germline cells (Figure 1A-A', arrows), and in the hub, an organizing center and stem cell niche in the *Drosophila* testis (Figure 1A''-A''', arrows)[33]. LD were largely absent from the testis region occupied by spermatocytes (Figure 1A and A', arrowheads). While LD may contain multiple neutral lipid species[34], cholesterol-binding fluorescent polyene antibiotic filipin III did not detect cholesterol within testis LD (Figure S1A'), suggesting triglyceride is the main neutral lipid in *Drosophila* testis LD.

Drosophila spermatogenesis requires the codevelopment and differentiation of two cell lineages, the germline and the somatic cells[35]. To identify LD in each lineage, we used the GAL4/UAS system to overexpress a transgene in which GFP is fused to the LD-targeting motif of motor protein Klarsicht[36] (*UAS-GFP-LD*). We targeted *UAS-GFP-LD* to somatic cells with *Traffic jam* (*Tj*)-*GAL4* and to the germline using *nanos (nos)-GAL4*; LD were visualized using neutral lipid dye LipidTox. We found LD in the somatic cells of 0-day-old males (Figure 1D), and showed that the majority of somatic LD were <30 μm from the hub (Figure 1E). Because the somatic LD distribution coincided with a marker for somatic stem cells and their immediate daughter cells (Zinc

finger homeodomain 1, Zfh-1) (Figure 1F; two-sample Kolmogorov-Smirnov test)[37], but not with a marker for late somatic cells (Eyes absent, Eya)[38,39], our data suggests LD are present in early somatic cells. In the germline, GFP punctae corresponding to LD were found near the apical tip of the testis in 0-day-old males (Figure 1G,H). We found that the disappearance of germline LD coincided with peak expression of a GFP reporter that reflects the expression of Bag-of-marbles (Bam) protein in the testis (Bam-GFP)[40] (Figure 1I,1J). Because peak Bam expression signals the last round of transient amplifying mitotic cell cycle prior to the germline's transition into the meiotic cell cycle[41–43], our data suggests that germline LD, like somatic LD, are present at early stages of germline development.

brummer plays a cell-autonomous role in regulating testis lipid droplets

Adipose triglyceride lipase (*ATGL*) is a critical regulator of neutral lipid metabolism and LD[44–53]. Loss of *ATGL* in many cell types triggers LD accumulation, and *ATGL* overexpression decreases LD number[46,47,50,52,52,54–56]. Given that the *Drosophila ATGL* homolog *brummer* (*bmm*) regulates testis LD induced by mitochondrial stress[26], we explored whether *bmm* regulates testis LD under normal physiological conditions. We first examined *bmm* expression in the testis by isolating this organ from flies in which a *bmm* promoter fragment drives *GFP* expression (*bmm-GFP*). Indeed, *bmm-GFP* accurately reproduces changes to *bmm* mRNA levels[57]. GFP expression was present in the germline of *bmm-GFP* testes, and germline GFP levels were higher in spermatocytes than at earlier stages of sperm development (Figure 2A,2B; one-way ANOVA with Tukey multiple comparison test). Supporting this, our analysis of a publicly

89 available single-cell RNA sequencing data set of the male reproductive organ[58]
90 suggested a similar trend in *bmm* mRNA levels between different stages of germline
91 (Figure S2A,S2B) and somatic cell (Figure S2C,S2D) development. Importantly,
92 germline GFP levels were negatively correlated with testis LD in *bmm-GFP* flies (Figure
93 2A,2C), suggesting regions with higher *bmm* expression had fewer LD.
94 To test whether *bmm* regulates testis LD, we compared LD in testes from 0-day-
95 old males carrying a loss-of-function mutation in *bmm* (bmm^{1}) to control male testes
96 (bmm^{rev})[46]. bmm^{1} testes had significantly more LD across all LD sizes compared with
97 control males (Figure 2D–2G; Welch two-sample t-test with Bonferroni correction), and
98 showed a significantly expanded LD distribution (Figure 2D–2F,2H; two-sample
99 Kolmogorov-Smirnov test). This suggests *bmm* normally restricts LD to the region near
100 the apical tip of the testis, a role we confirm in both somatic and germline lineages
101 (Figure S2E–S2H). Importantly, after inducing homozygous bmm^{1} or bmm^{rev} clones in
102 the testes using *FLP-FRT* system[59], we found bmm^{1} spermatocyte clones had
103 significantly more LD at 3 days post-clone induction (Figure 2I; Welch two-sample t-
104 test), a stage at which LD were absent from bmm^{rev} clones. This indicates a previously
105 unrecognized cell-autonomous role for *bmm* in regulating testis LD, a role we were
106 unable to assess in somatic cells as we recovered no bmm^{1} somatic cell clones.
107

108 **_brummer_ plays a cell-autonomous role in regulating germline development**

109 To determine the physiological significance of *bmm*-mediated regulation of testis LD, we
110 investigated testis and sperm development in males without *bmm* function. In 0-day-old
111 bmm^{1} males reared at 25°C, testis size was significantly smaller than in age-matched

112 *bmm*^{rev} controls (Figure S3A; Welch two-sample t-test), and the number of spermatid
113 bundles was significantly lower (Figure S3B; Kruskal-Wallis rank sum test). Defects in
114 testis size and sperm development were also observed in 14-day-old *bmm*^{1} males
115 (Figure S3C,S3D Welch two-sample t-test). When the animals were reared at 29°C, a
116 temperature that exacerbates spermatogenesis defects associated with changes in lipid
117 metabolism[18], *bmm*^{1} phenotypes were more pronounced (Figure 3A-3C). This suggests
118 loss of *bmm* affects testis development and spermatogenesis. Because similar
119 phenotypes are observed in male mice without ATGL[32], and supplementing the diet of
120 *bmm*^{1} males with medium-chain triglycerides (MCT) partially rescues the testis and
121 spermatogenic defects we observed in flies (Figure S3E,S3F; one-way ANOVA with
122 Tukey multiple comparison test), as it does in mice[32,60], our data suggests flies are a
123 good model to study how *bmm*/*ATGL* influences sperm development.
124 To explore spermatogenesis in *bmm*^{1} animals, we used a germline-specific
125 marker Vasa to visualize the germline in the testes of *bmm*^{1} and *bmm*^{rev} males (Figure
126 3D,3E)[61]. We observed a significant increase in the number of germline stem cells
127 (GSC) (Figure 3F; Kruskal-Wallis rank sum test) and higher variability in GSC number in
128 *bmm*^{1} males (p=5.7×10^{-12} by F-test). Given that GSC number is affected by hub size
129 and GSC proliferation[62,63], we monitored both parameters in *bmm*^{1} and *bmm*^{rev} controls.
130 While hub size in *bmm*^{1} testes was significantly larger than in testes from *bmm*^{rev}
131 controls (Figure S3G,S3H; Welch two-sample t-test), the number of phosphohistone H3-
132 positive GSC, which indicates proliferating GSC, was unchanged in *bmm*^{1} animals
133 (Figure S3I; Kruskal-Wallis rank sum test). While this indicates a larger hub may partly
134 explain *bmm*'s effect on GSC number, *bmm* also plays a cell-autonomous role in

135 regulating GSC, as we recovered a higher proportion of *bmm*^{1} clones in the GSC pool
136 compared with *bmm*^{rev} clones at 14 days after clone induction (Figure 3G; Welch two-
137 sample t-test).

138 Beyond GSC, we uncovered additional spermatogenesis defects in *bmm*^{1} testes.
139 Peak Bam-GFP expression in testes from 0-day-old *bmm*^{1} and *bmm*^{rev} males showed
140 that GFP-positive cysts with were significantly further away from the hub in *bmm*^{1} testes
141 (Figure 3H,S3J; Welch two-sample t-test). Indeed, 15/18 *bmm*^{1} testes contained Vasa-
142 positive cysts with large nuclei in the distal half of the testis (Figure 3I, arrowheads), a
143 phenotype not present in *bmm*^{rev} testes (0/8) (p=0.0005 by Pearson's Chi-square test).
144 Because these phenotypes are also seen in testes with differentiation defects[10,64], we
145 recorded the stage of sperm development reached by the germline in *bmm*^{1} testes.
146 Most *bmm*^{1} testes contained post-meiotic cells in males raised at 25°C (Figure S3K);
147 however, germline development did not progress past the spermatocyte stage in most
148 *bmm*^{1} testes from animals raised at 29°C (Figure S3K). Testes from *bmm*^{1} males reared
149 at 25°C also had a smaller Boule-positive area (Figure 3J,S3L; Welch two-sample t-
150 test), and fewer individualization complexes and waste bags (Figure S3M,S3N; Kruskal-
151 Wallis rank sum test). Together, these data indicate loss of *bmm* delays germline
152 development. Because we recovered fewer *bmm*^{1} spermatocyte and spermatid clones
153 14 days after clone induction (Figure 3K,3L; Kruskal-Wallis rank sum test), this effect on
154 germline development represents a cell-autonomous role for *bmm*.
155

156 ***brummer*-dependent regulation of testis triglyceride levels affects**
157 **spermatogenesis**

158 *ATGL* catalyzes the first and rate-limiting step of triglyceride hydrolysis[52,65,66]. Loss of
159 this enzyme or its homologs leads to excess triglyceride accumulation[21,46,52,54,55] and
160 shifts in multiple lipid classes[45,67–69]. To determine how loss of *bmm* affects
161 spermatogenesis, we carried out mass spectrometry (MS)-based untargeted lipidomic
162 profiling of bmm^{1} and bmm^{rev} males. Hierarchical clustering of lipid species suggests
163 that bmm^{1} and bmm^{rev} males show distinct lipidomic profiles (Figure 4A). Overall, we
164 detected 2464 and 1144 lipid features with high quantitative confidence in positive and
165 negative ion modes, respectively. By matching experimental *m/z*, isotopic ratio, and
166 tandem MS spectra to lipid libraries, we confirmed 293 unique lipid species
167 (Supplemental table 1). We found 107 lipids had a significant change in abundance
168 between bmm^{1} and bmm^{rev} males ($p_{adj}<0.05$): 85 species were upregulated in bmm^{1}
169 males and 22 lipid species were downregulated. Among differentially regulated species
170 in different lipid classes, triglyceride had the largest residual above expected proportion
171 ($p=5.00\times10^{-4}$ by Pearson's Chi-squared test). This suggests triglyceride is the lipid class
172 most affected by loss of *bmm* (Figure 4B,4C).
173 In bmm^{1} males, most triglyceride species (55/97) were significantly higher.
174 Because we observed a positive correlation between the fold increase in triglyceride
175 abundance with both the number of double bonds ($p=7.52\times10^{-8}$ by Kendall's rank
176 correlation test; Figure S4A) and the number of carbons ($p=2.77\times10^{-10}$ by Kendall's rank
177 correlation test; Figure S4B), our data align well with *bmm*/*ATGL's* known role in
178 regulating triglyceride levels[46,47,52] and its substrate preference of long-chain
179 polyunsaturated fatty acids[65]. While we also detected changes in species such as fatty
180 acids, acylcarnitine, and membrane lipids (Figure S4C–S4H), in line with recent

181 *Drosophila* lipidomic data[70,71], the striking accumulation of triglyceride in *bmm*^{1} males
182 suggested that excess testis triglyceride in *bmm*^{1} males contributes to their
183 spermatogenic defects. To test this, we examined spermatogenesis in *bmm*^{1} males
184 carrying loss-of-function mutations in *midway* (*mdy*). *mdy* is the *Drosophila* homolog of
185 *diacylglycerol O-acyltransferase 1* (*DGAT1*), and whole-body loss of *mdy* reduces
186 whole-body triglyceride levels[72–74]. Importantly, testes isolated from males lacking both
187 *bmm* and *mdy* (genotype *mdy*$^{QX25/k03902}$*;bmm*^{1}) had fewer LD than testes dissected from
188 *bmm*^{1} males (Figures 4D,S4I; one-way ANOVA with Tukey multiple comparison test).
189 We found that testes isolated from *mdy*$^{QX25/k03902}$*;bmm*^{1} males were significantly
190 larger and had more spermatid bundles than testes from *bmm*^{1} males (Figure 4E–G;
191 one-way ANOVA with Tukey multiple comparison test). The elevated number of GSC in
192 *bmm*^{1} male testes was similarly rescued in *mdy*$^{QX25/k03902}$*;bmm*^{1} males (Figure 4H; one-
193 way ANOVA with Tukey multiple comparison test). These data suggest that defective
194 spermatogenesis in *bmm*^{1} males can be partly attributed to excess triglyceride
195 accumulation. Notably, at least some of these defects are cell-autonomous: RNAi-
196 mediated knockdown of *mdy* in the germline of *bmm*^{1} males partially rescued the
197 defects in testis size (Figure 4I; Kruskal-Wallis rank sum test with Dunn's multiple
198 comparison test) and GSC variance (Figure S4J; p=4.5 x 10^{-5} and 8.2 x 10^{-3} by F-test
199 from the GAL4- and UAS-only crosses, respectively). Thus, *bmm*-mediated regulation of
200 testis triglyceride plays a previously unrecognized role in regulating sperm development.
201 Overall, our study demonstrates a key role for neutral lipids, specifically
202 triglyceride, in supporting *Drosophila* sperm development. We further show that loss of
203 *bmm*, a key regulator of cellular triglyceride homeostasis, delays germline differentiation

204 leading to an accumulation of early-stage germ cells. While studies in mammals
205 suggest that testis lipid droplets contain cholesterol and play a role in promoting
206 steroidogenesis[75,76], we show that *bmm*-dependent regulation of triglyceride-containing
207 LD also influences sperm development. In nongonadal cell types, triglycerides are a rich
208 source of fatty acids for cellular ATP production, lipid building blocks to support
209 membrane homeostasis and growth, and metabolites that can act as signaling
210 molecules[77,78]. Because all of these factors support normal sperm development, future
211 studies will need to test how each factor contributes to the spermatogenic defects
212 caused by excess triglyceride accumulation. Further studies will also be needed to
213 identify the upstream signaling networks that regulate cellular triglyceride metabolism in
214 the testis. For example, the insulin/insulin-like growth factor signaling pathway, Target of
215 rapamycin pathway, and nuclear factor κB/Relish pathway influence *bmm* mRNA levels
216 in nongonadal cell types[79–85], and contribute to sperm development[9,14,86,87]. Given the
217 parallel spermatogenic defects we observed in *bmm*^{1} flies and *ATGL* knockout mice,
218 these follow-up studies will likely provide vital mechanistic insight into how neutral lipids
219 and triglycerides support spermatogenesis in other animals.

220 **ACKNOWLEDGEMENTS**

221 We thank Dr. Ronald Kühnlein for *bmm*[1] and *bmm*[rev] lines[46], Dr. Michael Welte for *UAS-*
222 *GFP-LD*[36], and Dr. Kaeko Kamei for *bmm-GFP*[57]. We used stocks from the Bloomington
223 *Drosophila* Stock Center (NIH P40OD018537) and Vienna *Drosophila* Resource Center
224 (VDRC). We acknowledge critical resources and information provided by FlyBase[88]
225 (supported by the National Human Genome Research Institute at the U.S. National
226 Institutes of Health (U41 HG000739) and the British Medical Research Council
227 (MR/N030117/1)). This work was supported by the Life Sciences Institutes Imaging
228 Core, supported by the UBC GREx Biological Resilience Initiative. Funding for this
229 study was provided by grants to EJR from the Canadian Institutes for Health Research
230 (PJT-153072), Michael Smith Foundation for Health Research (16876), and the
231 Canadian Foundation for Innovation (JELF-34879). GT was supported by a grant from
232 the Natural Sciences and Engineering Research Council (NSERC; 2018-04648),
233 TH/HY/CW were supported by NSERC (2020-04895), MA was supported by the
234 Jacob's foundation. We would like to acknowledge that our research takes place on the
235 traditional, ancestral, and unceded territory of the Musqueam people; a privilege for
236 which we are grateful.

237

238 **AUTHOR CONTRIBUTIONS**

239 Conceptualization, C.C. and E.J.R.; Methodology, C.C. and Y.Y.P.; Software, C.C.;
240 Investigation, C.C., H.Y., and Y.Y.P.; Lipidomics, M.A., H.Y., C.W., T.H.; Writing –
241 Original Draft, C.C. and E.J.R.; Writing – Review and Editing, C.C., E.J.R., and Y.Y.P.;

242 Supervision, E.J.R., G.T., and T.H.; Project administration, E.J.R.; Funding Acquisition,
243 E.J.R., G.T., and T.H.
244
245 **DECLARATION OF INTERESTS**
246 The authors declare no competing interests.
247
248 **FIGURE LEGENDS**
249 **Figure 1 – Lipid droplets are present in early-stage somatic and germ cells.** (A)
250 Testis lipid droplets (LD) in *w*^{1118} animals visualized with neutral lipid dye BODIPY.
251 (A,A') Scale bar=50 μm; (A'',A''') scale bar=15 μm. Asterisk indicates hub in all images.
252 Arrows point to LD; arrowheads point to spermatocytes in A,B. (B) Testis LD visualized
253 with BODIPY in newly-eclosed males. Scale bars: main image=50 μm; inset image=10
254 μm. (C) Testis LD from *w*^{1118} animals at different times post-eclosion. Scale bars=50
255 μm. (D) Testis LD visualized with LipidTox Red in animals with somatic cell
256 overexpression of GFP-LD (*Tj-GAL4>UAS-GFP-LD*). GFP- and LipidTox Red-positive
257 punctae are somatic LD (D–D''' arrows); LipidTox punctae without GFP indicate
258 germline LD (D–D''' arrowheads). Scale bars=10 μm. (E) Histogram showing the spatial
259 distribution of somatic cell LD; error bars represent standard error of the mean (SEM).
260 (F) Cumulative frequency distributions of somatic LD (blue line, data reproduced from
261 E), zfh-1-positive somatic cells (zfh-1^{+} cells, orange line), and Eya-positive somatic cells
262 (Eya^{+} cells, grey line). (G) Testis LD indicated by LipidTox Red in males with germline
263 overexpression of GFP-LD (*nos-GAL4>UAS-GFP-LD*). GFP- and LipidTox Red-positive
264 punctae indicate germline LD (arrows); LipidTox punctae without GFP indicate non-

265 germline LD (arrowheads). Scale bars=10 μm. (H) Histogram representing the spatial
266 distribution of LD within germline; error bars represent SEM. (I) Histogram representing
267 the spatial distribution of LD and GFP fluorescence (green line) (arbitrary units, a.u.) in
268 a representative testis of a *bam-GFP* animal (panel J). (J) Testis LD in a *bam-GFP*
269 animal. Scale bar=50 μm. See also Supplemental Figure 1.
270
271 **Figure 2 – *bmm* regulates testis lipid droplets in a cell-autonomous manner.** (A)
272 Testis lipid droplets (LD) indicated by LipidTox Red in *bmm-GFP* animals. Scale
273 bars=50 μm. Asterisks indicate the hub in all images. (B) Quantification of nuclear GFP
274 intensity in testes isolated from *bmm-GFP* animals (n=3). Germline stem cell (GSC),
275 spermatogonia (SG), spermatocyte (SC). (C) Spatial distribution of LD (grey histogram)
276 and GFP expression (green line) in testes from *bmm-GFP* animals as a function of
277 distance from the hub (n=3). (D,E) LD near the apical region of the testis in bmm^{rev} (D)
278 or bmm^{1} (E) animals.; (F) LD further away from the apical tip in bmm^{1} animals. (D–F)
279 Scale bars=50 μm. (G) Histogram representing testis LD size distribution in bmm^{rev}
280 (grey) and bmm^{1} (orange). (H) Apical tip of the testes is at the left of the graph;
281 individual dots represent a single LD and its relative position to the hub marked by an
282 asterisk. Cumulative frequency distribution of the distance between LDs and the apical
283 tip of the testes are drawn as solid lines. (I) Number of testis LD in bmm^{rev} (grey) or
284 bmm^{1} (orange) in FLP-FRT clones 3 days post-clone induction; dots represent
285 measurements from a single clone. The number of cells in each cyst (CC) counted is
286 indicated. See also Supplemental Figure 2.
287

288 **Figure 3 – A cell-autonomous role for *bmm* in regulating spermatogenesis.** Testes
289 isolated from *bmm*^{rev} (A) and *bmm*^{1} (A') animals raised at 29°C stained with phalloidin.
290 Scale bars=100 μm. (B) Testis size in *bmm*^{1} and *bmm*^{rev} animals raised at 29°C. (C)
291 Spermatid bundles in *bmm*^{1} and *bmm*^{rev} testes from animals reared at 29°C. (D,E)
292 Representative images of *bmm*^{rev} (D) or *bmm*^{1} (E) testes stained with DAPI and anti-
293 Vasa antibody. Arrows indicate germline stem cells (GSC). Scale bar=50 μm. The hub
294 is marked by an asterisk in all images. (F) GSC number in *bmm*^{1} and *bmm*^{rev} testes. (G)
295 Proportion of GSCs that were either *bmm*^{1} or *bmm*^{rev} clones at 3 and 14 days post-
296 clone induction. (H) Representative images of *bmm*^{rev} (H) and *bmm*^{1} (H') testes carrying
297 *bam-GFP*; data quantified in Figure S3J. Arrows indicate regions with high Bam-GFP.
298 Scale bars=50 μm. (I) Representative images of *bmm*^{rev} (I) or *bmm*^{1} (I',I'') testes stained
299 with anti-Vasa antibody. Arrows indicate Vasa-positive cysts in *bmm*^{1} testis. Panel I'' is
300 magnified from the boxed region in I'. (I,I') Scale bars=100 μm; (I'') scale bar=50 μm. (J)
301 Maximum projection of *bmm*^{rev} (J) or *bmm*^{1} (J') testes stained with anti-Boule antibody
302 (green) and DAPI (blue). Scale bars=100 μm. Number of *bmm*^{1} and *bmm*^{rev}
303 spermatocyte clones (K) or post-meiotic clones (L) at 14 days post-clone induction. See
304 also Supplemental Figure 3.
305
306 **Figure 4 – Loss of *bmm* disrupts triglyceride homeostasis and leads to**
307 **spermatogenic defects.** (A) Hierarchical clustering of lipid species detected in *bmm*^{rev}
308 and *bmm*^{1} animals. (B) Histograms showing the proportion of species in each lipid class
309 with different levels between *bmm*^{1} and *bmm*^{rev}. Numbers on histograms indicate the
310 number of species with differences in abundance. (C) Volcano plot showing fold change

311 in abundance of triglycerides (green; 97 species) and non-triglyceride lipids (grey; 186
312 species) in our dataset. (D) Arrows indicate testis LD stained with LipidTox Red in
313 *bmm*^{rev} (D), *bmm*^{1} (D'), or *mdy*$^{QX25/k03902}$; *bmm*^{1} (D'') animals. (E) Whole testes isolated
314 from *bmm*^{rev} (E), *bmm*^{1} (E'), or *mdy*$^{QX25/k03902}$;*bmm*^{1} (E'') animals stained with anti-Vasa
315 antibody (red) and DAPI (blue). Arrowheads indicate spermatid bundles. Scale
316 bars=100 μm. (F) Testis size in *bmm*^{rev}, *bmm*^{1}, and *mdy*$^{QX25/k03902}$;*bmm*^{1} animals.
317 Spermatid bundles (G) and number of germline stem cells (H) in *bmm*^{rev}, *bmm*^{1}, and
318 *mdy*$^{QX25/k03902}$;*bmm*^{1} animals. (I) Testis size in animals with germline-specific *mdy*
319 knockdown (*nos-GAL4>mdy RNAi*; *bmm*^{1}) compared with controls (*nos-GAL4*>+; *bmm*^{1}
320 and +>*mdy RNAi*; *bmm*^{1}). See also Supplemental Figure 4.
321

STAR METHODS

RESOURCE AVAILABILITY

Lead contact. Further information and requests for resources and reagents should be directed to, and will be fulfilled by, lead contact Dr. Elizabeth J. Rideout (elizabeth.rideout@ubc.ca).

Materials availability. *Drosophila* strains and their source are listed in the Key Resources table. Further information and requests for resources and reagents should be directed to, and will be fulfilled by, lead contact Dr. Elizabeth J. Rideout (elizabeth.rideout@ubc.ca).

Data and Code availability. All raw data and results of statistical tests reported in this paper are located in Supplementary files 1-4. This paper does not report original code. Any additional information required to reanalyze the data reported in this paper is available from the lead contact upon request.

EXPERIMENTAL MODEL AND SUBJECT DETAILS

Fly husbandry. Fly stocks were maintained at room temperature in 12:12 hour light:dark cycle. Unless otherwise indicated, all flies were raised at 25°C with a density of 50 larvae per 10 mL fly media. Because this project examines sperm development, we used male flies in all experiments. Fly media contained 20.5 g of sucrose (SU10,

345 Snow Cap), 70.9 g of Dextrose (SUG8, Snow Cap), 48.5 g of cornmeal (AO18006,
346 Snow Cap), 30.3 g of baker's yeast (NB10, Snow Cap), 4.55 g of agar (DR-820-25F,
347 SciMart), 0.5 g of calcium chloride dihydrate (CCL302.1, BioShop Canada), 0.5 g of
348 magnesium sulfate heptahydrate (MAG511.1, BioShop Canada), 4.9 mL of propionic
349 acids (P1386, Sigma-Aldrich), and 488 µL of phosphoric acid (P5811, Sigma-Aldrich)
350 per 1L of media. For diets with medium- or long-chain triglyceride, 4 g of coconut oil
351 (medium chain triglyceride) or olive oil (long chain triglyceride) was added per 100 mL of
352 media described above prior to cooling. Males were collected and dissected within 24
353 hours of eclosion unless otherwise indicated. Fixations were performed at room
354 temperature with 4% paraformaldehyde (CA11021-168, VWR) in PBS for 20 minutes on
355 a rotating platform followed by washing in PBS twice before staining. Fly strains used in
356 our study are listed in the Key Resources table.
357
358 **METHOD DETAILS**
359
360 **Testis cell stage classification and measurements.** Cells at an early stage of
361 development (stem cells and early-stage somatic and germline cells) were located in
362 the apical region of the testis, and were identified by their small and dense nuclei[89].
363 GSC were defined as Vasa-positive cells in direct contact with the hub; proliferating
364 GSC were identified as Vasa-positive cells in direct contact with the hub that were also
365 phospho-H3 positive. Cells in the testis region occupied by primary spermatocytes were
366 identified by their large cell size and decondensed chromosome staining occupying
367 three nuclear domains[89]. Spermatid bundles were identified by their condensed and

368 needle-shaped nuclei, which roughly corresponds to nuclei with protamine-based
369 chromatin[3]. Testis size was measured by quantifying the length of a line drawn down
370 the middle of a testis image; starting from the apical tip of the testis and ending where
371 the testis meets the seminal vesicle.
372
373 ***FLP-FRT clone induction.*** Adult males were collected at 3-5 days post-eclosion and
374 heat-shocked three times at 37°C with a 10 min rest period at room temperature
375 between heat-shocks. After heat-shock, the flies were incubated at room temperature
376 until dissection.
377
378 ***Immunohistochemistry.*** Fixed samples were rinsed three times with blocking solution
379 containing 0.2% bovine serum albumin (A4503, Sigma-Aldrich), 0.3% Triton-X in PBS,
380 then blocked for 1 hr in PBS on a rotating platform at room temperature. During the
381 incubation, the blocking solution was changed every 15 minutes. After blocking, the
382 sample were resuspended in blocking solution with the appropriate concentration of
383 primary antibody (see Key Resources table), and incubated overnight at 4°C. Samples
384 were rinsed three times with blocking solution after removing primary antibody, and
385 blocked for one hour on a rotating platform in blocking solution. Secondary antibody
386 was applied in blocking solution and left on the rotating platform at room temperature for
387 40 min. The sample was then rinsed with blocking solution three more times, and
388 washed four times for 15 min per wash in blocking solution. Testis samples were
389 resuspended in Vectashield mounting media with DAPI (H-1200-10, Vector Laboratory)

390 or SlowFade Diamond mounting media (S36972, Thermo Fisher Scientific) prior to
391 mounting.
392
393 ***Lipid droplet staining.*** Fixed testes were briefly permeabilized with 0.1% Triton-X in
394 PBS for 5 min prior to applying phalloidin. For BODIPY staining, samples were
395 suspended in PBS containing 10 µg/mL DAPI (2879083-5mg, PeproTech), 1:500
396 BODIPY 495/503 (Thermo Fisher Scientific D3922), and 1:1000 phalloidin iFluor647
397 (ab176759, Abcam) or 1:40 phalloidin TexasRed (T7471, Thermo Fisher Scientific). For
398 staining with LipidTox Red, samples were suspended in PBS containing 10 µg/mL DAPI
399 (2879083-5mg, PeproTech), 1:200 LipidTox Red (H34476, Thermo Fisher Scientific),
400 and 1:1000 phalloidin iFluor647 (ab176759, Abcam). For staining free sterols, samples
401 were prepared as for BODIPY staining with 50 µg/mL filipin in place of BODIPY for 30
402 min. Samples were incubated on a rotating platform for 40 minutes at room
403 temperature. After incubation, samples were washed twice with PBS, then resuspended
404 in SlowFade Diamond mounting media (Thermo Fisher Scientific S36972) prior to
405 mounting.
406
407 ***Image acquisition and processing.*** All images were acquired on a Leica SP5 confocal
408 microscope system with 20X or 40X objectives and subsequently quantified with Fiji
409 image analysis software[90].
410
411 ***Drosophila lipidomics.*** *Drosophila* extracts were prepared following the previously
412 reported protocol[91]. Briefly, 10 *Drosophila* males (~10 mg) were weighed, 300 µL of ice-

413 cold methanol/water mixture (9:1, v:v) was added to these males, and the samples were
414 homogenized with glass beads using a bead beater (mini-beadbeater-16, BioSpec,
415 Bartlesville, Ok, USA). Sample weight was used for sample normalization. Fly lysate
416 was kept at -20°C for 4 hours for protein precipitation. Then, 900 μL of methyl tert-butyl
417 ether was added and the solution was shaken for 5 min to extract lipids. To induce
418 phase separation 285 μL of water was added, followed by centrifugation. The upper
419 layer was separated, dried, and reconstituted in isopropanol/acetonitrile (1:1, v:v) for
420 liquid chromatography-mass spectrometry (LC-MS) analysis. The volume of
421 reconstitution solution was proportional to sample weight for normalization. Quality
422 control (QC) samples were prepared by pooling 20 μL aliquot from each sample. The
423 method blank sample was prepared using an identical workflow but without adding
424 *Drosophila*.

425 *Drosophila* extracts were analyzed on an UHR-QqTOF (Ultra-High Resolution
426 Qq-Time-Of-Flight) mass spectrometry Impact II (Bruker Daltonics, Bremen, Germany)
427 interfaced with an Agilent 1290 Infinity II LC Systems (Agilent Technologies, Santa
428 Clara, CA, USA). LC separation was performed using a Waters reversed-phase (RP)
429 UPLC Acquity BEH C18 Column (1.7 μm, 1.0 mm ×100 mm, 130 Å) (Milford, MA, USA)
430 maintained at 30°C. For positive ion mode, the mobile phase A was 60% acetonitrile in
431 water and the mobile phase B was 90% isopropanol in acetonitrile, both containing 5
432 mM ammonium formate (pH = 4.8, adjusted by formic acid). For negative ion mode, the
433 mobile phase A was 60% acetonitrile in water and the mobile phase B was 90%
434 isopropanol in acetonitrile, both containing 5 mM NH_4FA (pH = 9.8, adjusted by
435 ammonium hydroxide). The LC gradient for positive and negative ion modes was set as

436 follow: 0 min, 5% B; 8 min, 40% B; 14 min, 70% B; 20 min, 95% B; 23 min, 95% B; 24
437 min, 5% B; 33 min, 5% B. The flow rate was 0.1 mL/min. The injection volume was
438 optimized to 2 μL in positive mode and 5 μL in negative mode using QC sample. The
439 ESI source conditions were set as follows: dry gas temperature, 220 °C; dry gas flow, 7
440 L/min; nebulizer gas pressure, 1.6 bar; capillary voltage, 4500 V for positive mode and
441 3000 V for negative mode. The MS1 analysis was conducted using following
442 parameters: mass range, 70-1000 m/z; spectrum type: centroid, calculated using
443 maximum intensity; absolute intensity threshold: 250. Data-dependent MS/MS analysis
444 parameters: collision energy: 16-30 eV; cycle time, 3 s; spectra rate: 4 Hz when
445 intensity < 10^4 and 12 Hz when intensity > 10^5, linearly increased from 10^4 to 10^5.
446 External calibration was applied using sodium formate to ensure the m/z accuracy
447 before sample analysis.
448 The raw LC-MS data were processed using MS-DIAL (ver. 4.38)[92]. The detailed
449 MS-DIAL parameters are: MS1 tolerance, 0.01 Da; MS/MS tolerance, 0.05; mass slice
450 width, 0.05 Da; smoothing method, linear weighted moving average; smoothing level, 3
451 scans; minimum peak width, 5 scans. Lipid features with high quantitative confidence
452 were selected by the following criteria: retention time was within the gradient elution
453 time (< 23 min); average intensity in QC samples is larger than 5-fold of the intensity in
454 method blank sample. Lipid identification was performed by matching experimental
455 precursor m/z, isotopic ratio and MS/MS spectrum against the LipidBlast libraries
456 embedded in MS-DIAL. To improve the quantification accuracy, the measured MS
457 signal intensities were corrected using serial diluted QC samples following the reported
458 workflow[93].

459

460 **QUANTIFICATION AND STATISTICAL ANALYSIS**

461

462 All microscopy images were quantified using Fiji software[90]. For lipid droplet counts, a
463 single optical slice through the middle of the testis containing the hub was used with the
464 exception of FLP-FRT experiment where all lipid droplets within a GFP-negative cyst
465 were counted (Figure 2I).

466

467 All statistical analyses were done using R (obtained from https://cran.r-project.org). With
468 exception of data concerning spatial distribution, and lipidomic data, Shapiro-Wilk test
469 (via *shapiro.test* in base R) was used to assess normality of distribution prior to testing
470 for significance. Kruskal-Wallis rank sum test (from the R package *coin*) and Dunn's test
471 (from the R package *dunn.test*) were used in place of Welch two-sample t-test and
472 Tukey's multiple comparison test when the assumption of normality was not met. For
473 testing differences in variance between two populations, F-test (via *var.test* in base R)
474 was used. For testing differences in spatial distribution, two-sample Kolmogorov-
475 Smirnov test (via *ks.test* in base R) was used. All *p*-values are indicated in figures;
476 extremely small *p*-values are listed as $p<2.2 \times 10^{-16}$.

477

478 **SUPPLEMENTAL TABLE AND FILES**

479 **Supplemental table 1** – Table showing identified lipid species from untargeted
480 lipidomic analysis.

481 **Supplementary file 1** – Raw data and statistical outputs from Figure 1.

482 **Supplementary file 2** – Raw data and statistical outputs from Figure 2 and

483 Supplemental figure 2.

484 **Supplementary file 3** – Raw data and statistical outputs from Figure 3 and

485 Supplemental figure 3.

486 **Supplementary file 4** – Raw data and statistical outputs from Figure 4 and

487 Supplemental figure 4.

REFERENCES

1. de Cuevas, M., and Matunis, E.L. (2011). The stem cell niche: lessons from the Drosophila testis. Dev. Camb. Engl. *138*, 2861–2869. 10.1242/dev.056242.

2. Demarco, R.S., Eikenes, Å.H., Haglund, K., and Jones, D.L. (2014). Investigating spermatogenesis in Drosophila melanogaster. Methods San Diego Calif *68*, 218–227. 10.1016/j.ymeth.2014.04.020.

3. Fabian, L., and Brill, J.A. (2012). Drosophila spermiogenesis. Spermatogenesis *2*, 197–212. 10.4161/spmg.21798.

4. Brill, J.A., Yildirim, S., and Fabian, L. (2016). Phosphoinositide signaling in sperm development. Semin. Cell Dev. Biol. *59*, 2–9. 10.1016/j.semcdb.2016.06.010.

5. Brill, J.A., Hime, G.R., Scharer-Schuksz, M., and Fuller, M.T. (2000). A phospholipid kinase regulates actin organization and intercellular bridge formation during germline cytokinesis. Development *127*, 3855.

6. Giansanti, M.G., Bonaccorsi, S., Kurek, R., Farkas, R.M., Dimitri, P., Fuller, M.T., and Gatti, M. (2006). The Class I PITP Giotto Is Required for Drosophila Cytokinesis. Curr. Biol. *16*, 195–201. 10.1016/j.cub.2005.12.011.

7. Wong, R., Hadjiyanni, I., Wei, H.-C., Polevoy, G., McBride, R., Sem, K.-P., and Brill, J.A. (2005). PIP2 Hydrolysis and Calcium Release Are Required for Cytokinesis in Drosophila Spermatocytes. Curr. Biol. *15*, 1401–1406. 10.1016/j.cub.2005.06.060.

8. Wong, R., Fabian, L., Forer, A., and Brill, J.A. (2007). Phospholipase C and myosin light chain kinase inhibition define a common step in actin regulation during cytokinesis. BMC Cell Biol. *8*, 15. 10.1186/1471-2121-8-15.

9. Amoyel, M., Hillion, K.-H., Margolis, S.R., and Bach, E.A. (2016). Somatic stem cell differentiation is regulated by PI3K/Tor signaling in response to local cues. Dev. Camb. Engl. *143*, 3914–3925. 10.1242/dev.139782.

10. Fairchild, M.J., Islam, F., and Tanentzapf, G. (2017). Identification of genetic networks that act in the somatic cells of the testis to mediate the developmental program of spermatogenesis. PLOS Genet. *13*, e1007026. 10.1371/journal.pgen.1007026.

11. Inaba, M., Venkei, Z.G., and Yamashita, Y.M. (2015). The polarity protein Baz forms a platform for the centrosome orientation during asymmetric stem cell division in the Drosophila male germline. eLife *4*, e04960. 10.7554/eLife.04960.

12. Krahn, M.P., Klopfenstein, D.R., Fischer, N., and Wodarz, A. (2010). Membrane Targeting of Bazooka/PAR-3 Is Mediated by Direct Binding to Phosphoinositide Lipids. Curr. Biol. *20*, 636–642. 10.1016/j.cub.2010.01.065.

524 13. Papagiannouli, F., Berry, C.W., and Fuller, M.T. (2019). The Dlg Module and
525 Clathrin-Mediated Endocytosis Regulate EGFR Signaling and Cyst Cell-Germline
526 Coordination in the Drosophila Testis. Stem Cell Rep. *12*, 1024–1040.
527 10.1016/j.stemcr.2019.03.008.

528 14. Ueishi, S., Shimizu, H., and H. Inoue, Y. (2009). Male Germline Stem Cell Division
529 and Spermatocyte Growth Require Insulin Signaling in Drosophila. Cell Struct.
530 Funct. *34*, 61–69. 10.1247/csf.08042.

531 15. Phan, V.H., Herr, D.R., Panton, D., Fyrst, H., Saba, J.D., and Harris, G.L. (2007).
532 Disruption of Sphingolipid Metabolism Elicits Apoptosis-Associated Reproductive
533 Defects in Drosophila. Dev. Biol. *309*, 329–341. 10.1016/j.ydbio.2007.07.021.

534 16. Steinhauer, J., Gijón, M.A., Riekhof, W.R., Voelker, D.R., Murphy, R.C., and
535 Treisman, J.E. (2009). Drosophila Lysophospholipid Acyltransferases Are
536 Specifically Required for Germ Cell Development. Mol. Biol. Cell *20*, 5224–5235.
537 10.1091/mbc.e09-05-0382.

538 17. Szafer-Glusman, E., Giansanti, M.G., Nishihama, R., Bolival, B., Pringle, J., Gatti,
539 M., and Fuller, M.T. (2008). A Role for Very-Long-Chain Fatty Acids in Furrow
540 Ingression during Cytokinesis in Drosophila Spermatocytes. Curr. Biol. *18*, 1426–
541 1431. 10.1016/j.cub.2008.08.061.

542 18. Ben-David, G., Miller, E., and Steinhauer, J. (2015). Drosophila spermatid
543 individualization is sensitive to temperature and fatty acid metabolism.
544 Spermatogenesis *5*. 10.1080/21565562.2015.1006089.

545 19. Jung, A., Hollmann, M., and Schafer, M.A. (2007). The fatty acid elongase NOA is
546 necessary for viability and has a somatic role in Drosophila sperm development. J.
547 Cell Sci. *120*, 2924–2934. 10.1242/jcs.006551.

548 20. Walther, T.C., and Farese, R.V. (2012). Lipid Droplets and Cellular Lipid
549 Metabolism. Annu. Rev. Biochem. *81*, 687–714. 10.1146/annurev-biochem-061009-
550 102430.

551 21. Wat, L.W., Chao, C., Bartlett, R., Buchanan, J.L., Millington, J.W., Chih, H.J.,
552 Chowdhury, Z.S., Biswas, P., Huang, V., Shin, L.J., et al. (2020). A role for
553 triglyceride lipase brummer in the regulation of sex differences in Drosophila fat
554 storage and breakdown. PLOS Biol. *18*, e3000595. 10.1371/journal.pbio.3000595.

555 22. Bajpai, M., Gupta, G., and Setty, B.S. (1998). Changes in carbohydrate metabolism
556 of testicular germ cells during meiosis in the rat. Eur. J. Endocrinol. *138*, 322–327.
557 10.1530/eje.0.1380322.

558 23. Paniagua, R., Rodriguez, M.C., Nistal, M., Fraile, B., and Amat, P. (1987). Changes
559 in the lipid inclusion/Sertoli cell cytoplasm area ratio during the cycle of the human
560 seminiferous epithelium. Reproduction *80*, 335–341. 10.1530/jrf.0.0800335.

561 24. Mori, H., and Christensen, A.K. (1980). Morphometric analysis of Leydig cells in the
562 normal rat testis. J. Cell Biol. *84*, 340–354. 10.1083/jcb.84.2.340.

563 25. Kerr, J.B., and De Kretser, D.M. (1975). CYCLIC VARIATIONS IN SERTOLI CELL
564 LIPID CONTENT THROUGHOUT THE SPERMATOGENIC CYCLE IN THE RAT.
565 Reproduction *43*, 1–8. 10.1530/jrf.0.0430001.

566 26. Demarco, R.S., Uyemura, B.S., D'Alterio, C., and Jones, D.L. (2019). Mitochondrial
567 fusion regulates lipid homeostasis and stem cell maintenance in the Drosophila
568 testis. Nat. Cell Biol. *21*, 710–720. 10.1038/s41556-019-0332-3.

569 27. Casado, M.E., Pastor, O., Mariscal, P., Canfrán-Duque, A., Martínez-Botas, J.,
570 Kraemer, F.B., Lasunción, M.A., Martín-Hidalgo, A., and Busto, R. (2013). Hormone-
571 sensitive lipase deficiency disturbs the fatty acid composition of mouse testis.
572 Prostaglandins Leukot. Essent. Fatty Acids *88*, 227–233.
573 10.1016/j.plefa.2012.12.005.

574 28. El-Shehawi, A.M., El-Shazly, S., Ahmed, M., Alkafafy, M., Sayed, S., Farouk, S.,
575 Alotaibi, S.S., and Elseehy, M.M. (2020). Transcriptome Analysis of Testis from
576 HFD-Induced Obese Rats (Rattus norvigicus) Indicated Predisposition for Male
577 Infertility. Int. J. Mol. Sci. *21*, 6493. 10.3390/ijms21186493.

578 29. Wang, W., Wei, S., Li, L., Su, X., Du, C., Li, F., Geng, B., Liu, P., and Xu, G. (2015).
579 Proteomic analysis of murine testes lipid droplets. Sci. Rep. *5*, 12070.
580 10.1038/srep12070.

581 30. Chen, M., Wang, H., Li, X., Li, N., Xu, G., and Meng, Q. (2014). PLIN1 deficiency
582 affects testicular gene expression at the meiotic stage in the first wave of
583 spermatogenesis. Gene *543*, 212–219. 10.1016/j.gene.2014.04.021.

584 31. Hermo, L., Chung, S., Gregory, M., Smith, C.E., Wang, S.P., El-Alfy, M., Cyr, D.G.,
585 Mitchell, G.A., and Trasler, J. (2008). Alterations in the testis of hormone sensitive
586 lipase-deficient mice is associated with decreased sperm counts, sperm motility, and
587 fertility. Mol. Reprod. Dev. *75*, 565–577. 10.1002/mrd.20800.

588 32. Masaki, H., Kim, N., Nakamura, H., Kumasawa, K., Kamata, E., Hirano, K., and
589 Kimura, T. (2017). Long-chain fatty acid triglyceride (TG) metabolism disorder
590 impairs male fertility: a study using adipose triglyceride lipase deficient mice. MHR
591 Basic Sci. Reprod. Med. *23*, 452–460. 10.1093/molehr/gax031.

592 33. de Cuevas, M., and Matunis, E.L. (2011). The stem cell niche: lessons from the
593 Drosophila testis. Development *138*, 2861–2869. 10.1242/dev.056242.

594 34. Walther, T.C., Chung, J., and Jr, R.V.F. (2017). Lipid Droplet Biogenesis. Annu.
595 Rev. Cell Dev. Biol. *33*, 491–510. 10.1146/annurev-cellbio-100616-060608.

596 35. Boyle, M., and DiNardo, S. (1995). Specification, migration and assembly of the
597 somatic cells of the Drosophila gonad. Development *121*, 1815–1825.
598 10.1242/dev.121.6.1815.

599 36. Yu, Y.V., Li, Z., Rizzo, N.P., Einstein, J., and Welte, M.A. (2011). Targeting the
600 motor regulator Klar to lipid droplets. BMC Cell Biol. *12*, 9. 10.1186/1471-2121-12-9.

601 37. Leatherman, J.L., and DiNardo, S. (2008). Zfh-1 Controls Somatic Stem Cell Self-
602 Renewal in the Drosophila Testis and Nonautonomously Influences Germline Stem
603 Cell Self-Renewal. Cell Stem Cell *3*, 44–54. 10.1016/j.stem.2008.05.001.

604 38. Amoyel, M., Hillion, K.-H., Margolis, S.R., and Bach, E.A. (2016). Somatic stem cell
605 differentiation is regulated by PI3K/Tor signaling in response to local cues. Dev.
606 Camb. Engl. *143*, 3914. 10.1242/dev.139782.

607 39. Fabrizio, J.J., Boyle, M., and DiNardo, S. (2003). A somatic role for eyes absent
608 (eya) and sine oculis (so) in drosophila spermatocyte development. Dev. Biol. *258*,
609 117–128. 10.1016/S0012-1606(03)00127-1.

610 40. Chen, D., and McKearin, D.M. (2003). A discrete transcriptional silencer in the bam
611 gene determines asymmetric division of the Drosophila germline stem cell.
612 Development *130*, 1159–1170. 10.1242/dev.00325.

613 41. Insco, M.L., Leon, A., Tam, C.H., McKearin, D.M., and Fuller, M.T. (2009).
614 Accumulation of a differentiation regulator specifies transit amplifying division
615 number in an adult stem cell lineage. Proc. Natl. Acad. Sci. U. S. A. *106*, 22311–
616 22316. 10.1073/pnas.0912454106.

617 42. Chen, D., Wu, C., Zhao, S., Geng, Q., Gao, Y., Li, X., Zhang, Y., and Wang, Z.
618 (2014). Three RNA Binding Proteins Form a Complex to Promote Differentiation of
619 Germline Stem Cell Lineage in Drosophila. PLoS Genet. *10*.
620 10.1371/journal.pgen.1004797.

621 43. Gonczy, P., Matunis, E., and DiNardo, S. (1997). bag-of-marbles and benign gonial
622 cell neoplasm act in the germline to restrict proliferation during Drosophila
623 spermatogenesis. Development *124*, 4361–4371.

624 44. Athenstaedt, K., and Daum, G. (2003). YMR313c/TGL3 Encodes a Novel
625 Triacylglycerol Lipase Located in Lipid Particles of Saccharomyces cerevisiae*. J.
626 Biol. Chem. *278*, 23317–23323. 10.1074/jbc.M302577200.

627 45. Chitraju, C., Trötzmüller, M., Hartler, J., Wolinski, H., Thallinger, G.G., Haemmerle,
628 G., Zechner, R., Zimmermann, R., Köfeler, H.C., and Spener, F. (2013). The impact
629 of genetic stress by ATGL deficiency on the lipidome of lipid droplets from murine
630 hepatocytes. J. Lipid Res. *54*, 2185–2194. 10.1194/jlr.M037952.

631 46. Grönke, S., Mildner, A., Fellert, S., Tennagels, N., Petry, S., Müller, G., Jäckle, H.,
632 and Kühnlein, R.P. (2005). Brummer lipase is an evolutionary conserved fat storage
633 regulator in Drosophila. Cell Metab. *1*, 323–330. 10.1016/j.cmet.2005.04.003.

634 47. Haemmerle, G., Lass, A., Zimmermann, R., Gorkiewicz, G., Meyer, C., Rozman, J.,
635 Heldmaier, G., Maier, R., Theussl, C., Eder, S., et al. (2006). Defective Lipolysis and
636 Altered Energy Metabolism in Mice Lacking Adipose Triglyceride Lipase. Science
637 *312*, 734–737. 10.1126/science.1123965.

638 48. Haemmerle, G., Moustafa, T., Woelkart, G., Büttner, S., Schmidt, A., van de Weijer,
639 T., Hesselink, M., Jaeger, D., Kienesberger, P.C., Zierler, K., et al. (2011). ATGL-
640 mediated fat catabolism regulates cardiac mitochondrial function via PPAR-α and
641 PGC-1. Nat. Med. *17*, 1076–1085. 10.1038/nm.2439.

642 49. Huijsman, E., van de Par, C., Economou, C., van der Poel, C., Lynch, G.S.,
643 Schoiswohl, G., Haemmerle, G., Zechner, R., and Watt, M.J. (2009). Adipose
644 triacylglycerol lipase deletion alters whole body energy metabolism and impairs
645 exercise performance in mice. Am. J. Physiol.-Endocrinol. Metab. *297*, E505–E513.
646 10.1152/ajpendo.00190.2009.

647 50. Korbelius, M., Vujic, N., Sachdev, V., Obrowsky, S., Rainer, S., Gottschalk, B.,
648 Graier, W.F., and Kratky, D. (2019). ATGL/CGI-58-Dependent Hydrolysis of a Lipid
649 Storage Pool in Murine Enterocytes. Cell Rep. *28*, 1923-1934.e4.
650 10.1016/j.celrep.2019.07.030.

651 51. Kurat, C.F., Natter, K., Petschnigg, J., Wolinski, H., Scheuringer, K., Scholz, H.,
652 Zimmermann, R., Leber, R., Zechner, R., and Kohlwein, S.D. (2006). Obese Yeast:
653 Triglyceride Lipolysis Is Functionally Conserved from Mammals to Yeast *. J. Biol.
654 Chem. *281*, 491–500. 10.1074/jbc.M508414200.

655 52. Zimmermann, R., Strauss, J.G., Haemmerle, G., Schoiswohl, G., Birner-
656 Gruenberger, R., Riederer, M., Lass, A., Neuberger, G., Eisenhaber, F., Hermetter,
657 A., et al. (2004). Fat Mobilization in Adipose Tissue Is Promoted by Adipose
658 Triglyceride Lipase. Science *306*, 1383–1386. 10.1126/science.1100747.

659 53. Attané, C., Peyot, M.-L., Lussier, R., Poursharifi, P., Zhao, S., Zhang, D., Morin, J.,
660 Pineda, M., Wang, S., Dumortier, O., et al. (2016). A beta cell ATGL-
661 lipolysis/adipose tissue axis controls energy homeostasis and body weight via
662 insulin secretion in mice. Diabetologia *59*, 2654–2663. 10.1007/s00125-016-4105-2.

663 54. Grönke, S., Müller, G., Hirsch, J., Fellert, S., Andreou, A., Haase, T., Jäckle, H., and
664 Kühnlein, R.P. (2007). Dual Lipolytic Control of Body Fat Storage and Mobilization in
665 Drosophila. PLOS Biol. *5*, e137. 10.1371/journal.pbio.0050137.

666 55. Lee, J.H., Kong, J., Jang, J.Y., Han, J.S., Ji, Y., Lee, J., and Kim, J.B. (2014). Lipid
667 Droplet Protein LID-1 Mediates ATGL-1-Dependent Lipolysis during Fasting in
668 Caenorhabditis elegans. Mol. Cell. Biol. *34*, 4165–4176. 10.1128/MCB.00722-14.

669 56. Tuohetahuntila, M., Molenaar, M.R., Spee, B., Brouwers, J.F., Houweling, M.,
670 Vaandrager, A.B., and Helms, J.B. (2016). ATGL and DGAT1 are involved in the
671 turnover of newly synthesized triacylglycerols in hepatic stellate cells. J. Lipid Res.
672 *57*, 1162–1174. 10.1194/jlr.M066415.

673 57. Men, T.T., Thanh, D.N.V., Yamaguchi, M., Suzuki, T., Hattori, G., Arii, M., Huy, N.T.,
674 and Kamei, K. (2016). A *Drosophila* Model for Screening Antiobesity Agents.
675 BioMed Res. Int. *2016*, 1–10. 10.1155/2016/6293163.

676 58. Li, H., Janssens, J., Waegeneer, M.D., Kolluru, S.S., Davie, K., Gardeux, V.,
677 Saelens, W., David, F., Brbić, M., Leskovec, J., et al. (2021). Fly Cell Atlas: a single-
678 cell transcriptomic atlas of the adult fruit fly. 2021.07.04.451050.
679 10.1101/2021.07.04.451050.

680 59. Xu, T., and Rubin, G.M. (1993). Analysis of genetic mosaics in developing and adult
681 Drosophila tissues. Development *117*, 1223–1237.

682 60. Kim, N., Nakamura, H., Masaki, H., Kumasawa, K., Hirano, K., and Kimura, T.
683 (2017). Effect of lipid metabolism on male fertility. Biochem. Biophys. Res. Commun.
684 *485*, 686–692. 10.1016/j.bbrc.2017.02.103.

685 61. Lasko, P.F., and Ashburner, M. (1988). The product of the Drosophila gene vasa is
686 very similar to eukaryotic initiation factor-4A. Nature *335*, 611–617.
687 10.1038/335611a0.

688 62. Resende, L.P.F., Boyle, M., Tran, D., Fellner, T., and Jones, D.L. (2013). Headcase
689 Promotes Cell Survival and Niche Maintenance in the Drosophila Testis. PLoS ONE
690 *8*, e68026. 10.1371/journal.pone.0068026.

691 63. Kiger, A.A., White-Cooper, H., and Fuller, M.T. (2000). Somatic support cells restrict
692 germline stem cell self-renewal and promote differentiation. Nature *407*, 750–754.
693 10.1038/35037606.

694 64. Lin, T.Y., Viswanathan, S., Wood, C., Wilson, P.G., Wolf, N., and Fuller, M.T.
695 (1996). Coordinate developmental control of the meiotic cell cycle and spermatid
696 differentiation in Drosophila males. Development *122*, 1331–1341.

697 65. Eichmann, T.O., Kumari, M., Haas, J.T., Farese, R.V., Zimmermann, R., Lass, A.,
698 and Zechner, R. (2012). Studies on the substrate and stereo/regioselectivity of
699 adipose triglyceride lipase, hormone-sensitive lipase, and diacylglycerol-O-
700 acyltransferases. J. Biol. Chem. *287*, 41446–41457. 10.1074/jbc.M112.400416.

701 66. Schweiger, M., Schreiber, R., Haemmerle, G., Lass, A., Fledelius, C., Jacobsen, P.,
702 Tornqvist, H., Zechner, R., and Zimmermann, R. (2006). Adipose Triglyceride
703 Lipase and Hormone-sensitive Lipase Are the Major Enzymes in Adipose Tissue
704 Triacylglycerol Catabolism *. J. Biol. Chem. *281*, 40236–40241.
705 10.1074/jbc.M608048200.

706 67. Missaglia, S., Maggi, L., Mora, M., Gibertini, S., Blasevich, F., Agostoni, P., Moro, L.,
707 Cassandrini, D., Santorelli, F.M., Gerevini, S., et al. (2017). Late onset of neutral
708 lipid storage disease due to novel PNPLA2 mutations causing total loss of lipase
709 activity in a patient with myopathy and slight cardiac involvement. Neuromuscul.
710 Disord. *27*, 481–486. 10.1016/j.nmd.2017.01.011.

711 68. Williams, M.L., Coleman, R.A., Placezk, D., and Grunfeld, C. (1991). Neutral lipid
712 storage disease: a possible functional defect in phospholipid-linked triacylglycerol
713 metabolism. Biochim. Biophys. Acta BBA - Mol. Basis Dis. *1096*, 162–169.
714 10.1016/0925-4439(91)90055-E.

715 69. Yang, L., Liang, J., Lam, S.M., Yavuz, A., Shui, G., Ding, M., and Huang, X. (2020).
716 Neuronal lipolysis participates in PUFA-mediated neural function and
717 neurodegeneration. EMBO Rep. *21*. 10.15252/embr.202050214.

718 70. Nazario-Yepiz, N.O., Fernández Sobaberas, J., Lyman, R., Campbell, M.R.,
719 Shankar, V., Anholt, R.R.H., and Mackay, T.F.C. (2021). Physiological and
720 metabolomic consequences of reduced expression of the Drosophila brummer
721 triglyceride Lipase. PLOS ONE *16*, e0255198. 10.1371/journal.pone.0255198.

722 71. Giedt, M.S., Thomalla, J.M., Johnson, M.R., Lai, Z.W., Tootle, T.L., and Welte, M.A.
723 (2021). Adipose triglyceride lipase promotes prostaglandin-dependent actin
724 remodeling by regulating substrate release from lipid droplets (Cell Biology)
725 10.1101/2021.08.02.454724.

726 72. Beller, M., Bulankina, A.V., Hsiao, H.-H., Urlaub, H., Jäckle, H., and Kühnlein, R.P.
727 (2010). PERILIPIN-Dependent Control of Lipid Droplet Structure and Fat Storage in
728 Drosophila. Cell Metab. *12*, 521–532. 10.1016/j.cmet.2010.10.001.

729 73. Buszczak, M., Lu, X., Segraves, W.A., Chang, T.Y., and Cooley, L. (2002).
730 Mutations in the midway Gene Disrupt a Drosophila Acyl Coenzyme A:
731 Diacylglycerol Acyltransferase. Genetics *160*, 1511–1518.

732 74. Martínez, B.A., Hoyle, R.G., Yeudall, S., Granade, M.E., Harris, T.E., Castle, J.D.,
733 Leitinger, N., and Bland, M.L. (2020). Innate immune signaling in Drosophila shifts
734 anabolic lipid metabolism from triglyceride storage to phospholipid synthesis to
735 support immune function. PLOS Genet. *16*, e1009192.
736 10.1371/journal.pgen.1009192.

737 75. Freeman, D.A., and Ascoli, M. (1982). Studies on the source of cholesterol used for
738 steroid biosynthesis in cultured Leydig tumor cells. J. Biol. Chem. *257*, 14231–
739 14238.

740 76. Wang, F., Chen, Z., Ren, X., Tian, Y., Wang, F., Liu, C., Jin, P., Li, Z., Zhang, F.,
741 and Zhu, B. (2017). Hormone-sensitive lipase deficiency alters gene expression and
742 cholesterol content of mouse testis. Reproduction *153*, 175–185. 10.1530/REP-16-
743 0484.

744 77. Walther, T.C., and Farese, R.V. (2012). Lipid droplets and cellular lipid metabolism.
745 Annu Rev Biochem *81*, 687–714. 10.1146/annurev-biochem-061009-102430.

746 78. Olzmann, J.A., and Carvalho, P. (2019). Dynamics and functions of lipid droplets.
747 Nat. Rev. Mol. Cell Biol. *20*, 137–155. 10.1038/s41580-018-0085-z.

748 79. Birse, R.T., Choi, J., Reardon, K., Rodriguez, J., Graham, S., Diop, S., Ocorr, K.,
749 Bodmer, R., and Oldham, S. (2010). High-fat-diet-induced obesity and heart
750 dysfunction are regulated by the TOR pathway in Drosophila. Cell Metab *12*, 533–
751 544. 10.1016/j.cmet.2010.09.014.

752 80. Molaei, M., Vandehoef, C., and Karpac, J. (2019). NF-κB Shapes Metabolic
753 Adaptation by Attenuating Foxo-Mediated Lipolysis in Drosophila. Dev. Cell *49*, 802-
754 810.e6. 10.1016/j.devcel.2019.04.009.

755 81. Alic, N., Andrews, T.D., Giannakou, M.E., Papatheodorou, I., Slack, C., Hoddinott,
756 M.P., Cocheme, H.M., Schuster, E.F., Thornton, J.M., and Partridge, L. (2011).
757 Genome-wide dFOXO targets and topology of the transcriptomic response to stress
758 and insulin signalling. Mol Syst Biol *7*, 502. 10.1038/msb.2011.36.

759 82. Junger, M.A., Rintelen, F., Stocker, H., Wasserman, J.D., Vegh, M., Radimerski, T.,
760 Greenberg, M.E., and Hafen, E. (2003). The Drosophila forkhead transcription factor
761 FOXO mediates the reduction in cell number associated with reduced insulin
762 signaling. J Biol *2*, 20. 10.1186/1475-4924-2-20.

763 83. Zinke, I., Schutz, C.S., Katzenberger, J.D., Bauer, M., and Pankratz, M.J. (2002).
764 Nutrient control of gene expression in Drosophila: microarray analysis of starvation
765 and sugar-dependent response. EMBO J *21*, 6162–6173.

766 84. Puig, O., and Tjian, R. (2005). Transcriptional feedback control of insulin receptor by
767 dFOXO/FOXO1. Genes Dev. *19*, 2435–2446. 10.1101/gad.1340505.

768 85. Kang, P., Chang, K., Liu, Y., Bouska, M., Birnbaum, A., Karashchuk, G., Thakore,
769 R., Zheng, W., Post, S., Brent, C.S., et al. (2017). Drosophila Kruppel homolog 1
770 represses lipolysis through interaction with dFOXO. Sci. Rep. *7*, 16369.
771 10.1038/s41598-017-16638-1.

772 86. Amoyel, M., Simons, B.D., and Bach, E.A. (2014). Neutral competition of stem cells
773 is skewed by proliferative changes downstream of Hh and Hpo. EMBO J. *33*, 2295–
774 2313. 10.15252/embj.201387500.

775 87. Hof-Michel, S., Cigoja, L., Huhn, S., and Bökel, C. (2020). Innate immune signalling
776 drives loser cell elimination during stem cell competition in the *Drosophila* testis
777 (Developmental Biology) 10.1101/2020.03.05.979161.

778 88. Thurmond, J., Goodman, J.L., Strelets, V.B., Attrill, H., Gramates, L.S., Marygold,
779 S.J., Matthews, B.B., Millburn, G., Antonazzo, G., Trovisco, V., et al. (2018).

780 FlyBase 2.0: the next generation. Nucleic Acids Res. *47*, D759–D765.
781 10.1093/nar/gky1003.

782 89. White-Cooper, H. (2004). Spermatogenesis. In Drosophila Cytogenetics Protocols
783 Methods in Molecular Biology., D. S. Henderson, ed. (Humana Press), pp. 45–75.
784 10.1385/1-59259-665-7:45.

785 90. Schindelin, J., Arganda-Carreras, I., Frise, E., Kaynig, V., Longair, M., Pietzsch, T.,
786 Preibisch, S., Rueden, C., Saalfeld, S., Schmid, B., et al. (2012). Fiji: an open-
787 source platform for biological-image analysis. Nat. Methods *9*, 676–682.
788 10.1038/nmeth.2019.

789 91. Yu, H., Villanueva, N., Bittar, T., Arsenault, E., Labonté, B., and Huan, T. (2020).
790 Parallel metabolomics and lipidomics enables the comprehensive study of mouse
791 brain regional metabolite and lipid patterns. Anal. Chim. Acta *1136*, 168–177.
792 10.1016/j.aca.2020.09.051.

793 92. Tsugawa, H., Cajka, T., Kind, T., Ma, Y., Higgins, B., Ikeda, K., Kanazawa, M.,
794 VanderGheynst, J., Fiehn, O., and Arita, M. (2015). MS-DIAL: data-independent
795 MS/MS deconvolution for comprehensive metabolome analysis. Nat. Methods *12*,
796 523–526. 10.1038/nmeth.3393.

797 93. Yu, H., and Huan, T. (2021). Patterned Signal Ratio Biases in Mass Spectrometry-
798 Based Quantitative Metabolomics. Anal. Chem. *93*, 2254–2262.
799 10.1021/acs.analchem.0c04113.

800

801 **SUPPLEMENTAL FIGURE LEGENDS**

802 **Supplemental Figure 1 related to Figure 1 – Cholesterol is absent from testis lipid**
803 **droplets.** (A) Testes stained with BODIPY (A) to detect neutral lipids and Filipin III (A')
804 to detect free cholesterol. Scale bars=50 μm.

805

806 **Supplemental Figure 2 related to Figure 2 – *bmm* mRNA levels during**
807 **spermatogenesis in germline and somatic lineages.** (A) Pseudotime trajectory of
808 germline (black line) based on single-cell RNA sequencing data[62]. Individual cells are
809 labeled according to the annotation within the data set. (B) Rolling average of
810 normalized *bmm* transcript counts in the germline along the trajectory shown in panel A

811 are plotted as a black line on the upper panel. Composition of cell types mapped on to
812 the trajectory at each time point is shown at the lower half of panel B. (C) Pseudotime
813 trajectory of the somatic cells (black line) based on publicly available single-cell RNA
814 sequencing data[62]. Individual cells are labeled according to the annotation within the
815 data set. (D) Rolling average of normalized *bmm* transcript counts in somatic cells
816 plotted as a black line along the trajectory shown in C (upper panel). Composition of cell
817 types mapped on to the trajectory at each time point (lower panel). (E-H)
818 Representative images of bmm^{rev} (E and F) and bmm^{1} (G and H) testes with somatic
819 over-expression of *GFP-LD* (*Tj-GAL4>UAS-GFP-LD*). Panel F and H contain magnified
820 images of the area indicated by the boxes in panel E and G, respectively. In bmm^{rev}
821 testes, LD were restricted to a region near the apical tip (E) of the testis in both somatic
822 (F–F''' arrows) and germline cells (F–F''' arrowheads). In bmm^{1} testes, LD were present
823 in both somatic (G–H arrows) and germline cells (G–H arrowheads), near the apical tip
824 of the testis in a region corresponding to early-stage germ cells, and in the region
825 corresponding to spermatocytes (G arrows and arrowheads, and H). Scale bars=50 μm;
826 (F and H) scale bars=20 μm.
827
828 **Supplemental Figure 3 related to Figure 3 – Additional characterization of testis**
829 **development and spermatogenesis in animals lacking *bmm*.** (A) Testis size was
830 smaller in bmm^{1} mutant animals compared with bmm^{rev} controls at <24 hr post-eclosion
831 when raised at 25°C (A; Welch two-sample t-test). (B) The number of spermatid bundles
832 was significantly lower in bmm^{1} mutant animals compared with bmm^{rev} controls at <24
833 hr post-eclosion when raised at 25°C (Kruskal-Wallis rank sum test). (C) Testis size was

834 significantly smaller in *bmm*^{1} mutant males compared with *bmm*^{rev} control males at 14-
835 days post-eclosion (Welch two sample t-test). (D) The median number of spermatid
836 bundles was not significantly different between *bmm*^{1} mutant males and *bmm*^{rev} control
837 males at 14 days post-eclosion (Welch two sample t-test), but 8/27 *bmm*^{1} testis had no
838 spermatid bundles, a phenotype we did not observe in age-matched *bmm*^{rev} males
839 (0/22) (p=0.0163, Pearson's Chi-squared test). (E) Food supplemented with 4% medium
840 chain triglyceride (MCT), but not long chain triglyceride (LCT), significantly increased
841 testis length in *bmm*^{1} animals but had no effect on this phenotype in *bmm*^{rev} control
842 animals (one-way ANOVA with Tukey multiple comparison test). (F) Food
843 supplemented with 4% medium chain triglyceride significantly increased the number of
844 spermatid bundles in *bmm*^{1} testes but had no effect on this phenotype in *bmm*^{rev} control
845 animals (one-way ANOVA with Tukey multiple comparison test). (G) Representative
846 images of *bmm*^{rev} (G–G') or *bmm*^{1} (G''–G''') testes stained for Fas3 (G and G'') and Vas
847 (G' and G'''). Scale bars = 25 μm. (H) Quantification of hub area in *bmm*^{rev} or *bmm*^{1}
848 testes showed a significantly larger hub size in *bmm*^{1} testes (Welch two-sample t-test).
849 (I) The number of germline stem cells undergoing mitosis (phospho-histone H3^{+}
850 GSC/total GSC) was not significantly different between *bmm*^{1} and *bmm*^{rev} testes
851 (Kruskal-Wallis rank sum test). (J) The distance between the hub and the first Bam-GFP
852 positive cyst (Figure 3H) was significantly higher in *bmm*^{1} testes than in *bmm*^{rev} testes
853 (Welch two-sample t-test). (K) All *bmm*^{rev} testes and most *bmm*^{1} testes contained
854 spermatids when raised at 25°C; however, the most advanced stage of
855 spermatogenesis observed in the majority of *bmm*^{1} testes isolated from animals reared
856 at 29°C was the spermatocyte stage. (L) Testes isolated from *bmm*^{1} animals contained

857 significantly less Boule-positive area than control testes (Welch two-sample t-test). (M)
858 Testes isolated from *bmm*^{1} animals contain fewer individualization complexes than
859 *bmm*^{rev} control testes (Kruskal-Wallis rank sum test). (N) Fewer waste bags were
860 present in testes isolated from *bmm*^{1} animals compared with *bmm*^{rev} control testes
861 (Kruskal-Wallis rank sum test).
862
863 **Supplemental Figure 4 related to Figure 4 – Lipidomic analysis of animals lacking**
864 ***bmm*.** (A) Higher fold-changes of triglycerides in *bmm*^{1} animals were associated with
865 less saturation in the acyl-groups (Kendall's rank correlation test). (B) Higher fold-
866 changes of triglycerides in *bmm*^{1} animals were associated with higher number of
867 carbons in the acyl-groups (Kendall's rank correlation test). Each dot represents a single
868 triglyceride species for panel B and C. (C) The volcano plot of identified lipids with
869 monoglycerides highlighted in blue and diglycerides highlighted in orange. Many
870 monoglycerides and diglycerides show increase in fold-change in *bmm*^{1} males. (D) The
871 number of carbon and the degree of saturation of monoglycerides (MAG) and
872 diglycerides (DAG) with significant changes in abundance between *bmm*^{1} and *bmm*^{rev}
873 males. (E) The volcano plot of identified lipids with fatty acids highlighted in magenta
874 and acyl-carnitine highlighted in green. Many fatty acids show an increase in fold-
875 change while many acyl-carnitines show a decrease in fold-change in *bmm*^{1} males. (F)
876 The number of carbon and the degree of saturation of fatty acids (FA) and acyl-
877 carnitines (ACar) with significant changes in abundance between *bmm*^{1} and *bmm*^{rev}
878 males. (G) The volcano plot of identified lipids with membrane lipids highlighted in
879 yellow. (H) The number of carbon and the degree of saturation of membrane lipids with

880 significant changes in abundance between *bmm*^{1} and *bmm*^{rev} males. For panel H and I,
881 PC: phosphatidylcholine; PE: phosphatidylethanolamine; PI: phosphatidylinositol; LPC:
882 lysophosphatidylcholine; LPE: lysophosphatidylethanolamine; SM: sphingomyelin; PG:
883 phosphatidylglycerol. (I) Loss of *mdy* function rescued the high number of LD in *bmm*^{1}
884 testes to the level observed in *bmm*^{rev} testes (one-way ANOVA with Tukey multiple
885 comparison test). (J) Germline specific loss of *mdy* in *bmm*^{1} animals does not reduce
886 GSC numbers, but the variance in GSC number is significantly reduced compared to
887 controls (*nos-GAL4*>+; *bmm*^{1} vs *nos-GAL4*>*mdy RNAi*; *bmm*^{1}: p=4.5 × 10^{-5}; +>*mdy*
888 *RNAi*; *bmm*^{1} vs *nos-GAL4*>*mdy RNAi*; *bmm*^{1}: p=0.0082 by F-test).
889
890

891 **KEY RESOURCE TABLE**

REAGENT or RESOURCE	SOURCE	IDENTIFIER
Antibodies		
Anti-Vasa (1:200)	Gift from R. Lehman, MIT	
Anti-Eya (1:50)	Developmental Studies Hybridoma Bank (DSHB)	eya10H6
Anti-zfh1 (1:1000)	Gift from J. Skeath, WUSTL	
Anti-boule (1:1000)	Gift from S. Wasserman, UCSD	
Anti-phospho-histone H3 (1:1000)	Millipore Sigma	05-1354
Experimental models: *Drosophila melanogaster*		
w^{1118}	Bloomington *Drosophila* stock center	3605
CantonS	Bloomington *Drosophila* stock center	64349
OregonR		
bmm^{1}	Dr. R. Kühlein	
bmm^{rev}	Dr. R. Kühlein	
mdy[Qx25], cn[1], bw[1]/CyO, l(2)DTS513[1]	Bloomington *Drosophila* stock center	5095
y[1],w[67c23];P{lacW}Cse1[k03802],mdy[k03902]/CyO	Bloomington *Drosophila* stock center	10536
w[1118];P{GD1749}v6367 (UAS-mdy-RNAi)	Vienna *Drosophila* resource center	6367

REAGENT or RESOURCE	SOURCE	IDENTIFIER
nos-GAL4::VP16	Bloomington *Drosophila* stock center	7303
Tj-GAL4	Gift from D. Godt, University of Toronto	
c587-GAL4	Bloomington *Drosophila* stock center	67747
bam-GFP	[44]	
bmm-GFP	[40]	
GFP-LD	Dr. M. Welte	
P{neoFRT}82B, bmm[1]	This study	
P{neoFRT}82B, bmm[rev]	This study	
bam-GFP, bmm[1]	This study	
bam-GFP, bmm[rev]	This study	
Software and algorithms		
Fiji	https://imagej.net/software/fiji/	
R	https://cran.r-project.org	

892
893

Figure 1 – Lipid droplets are present in early-stage somatic and germline cells.

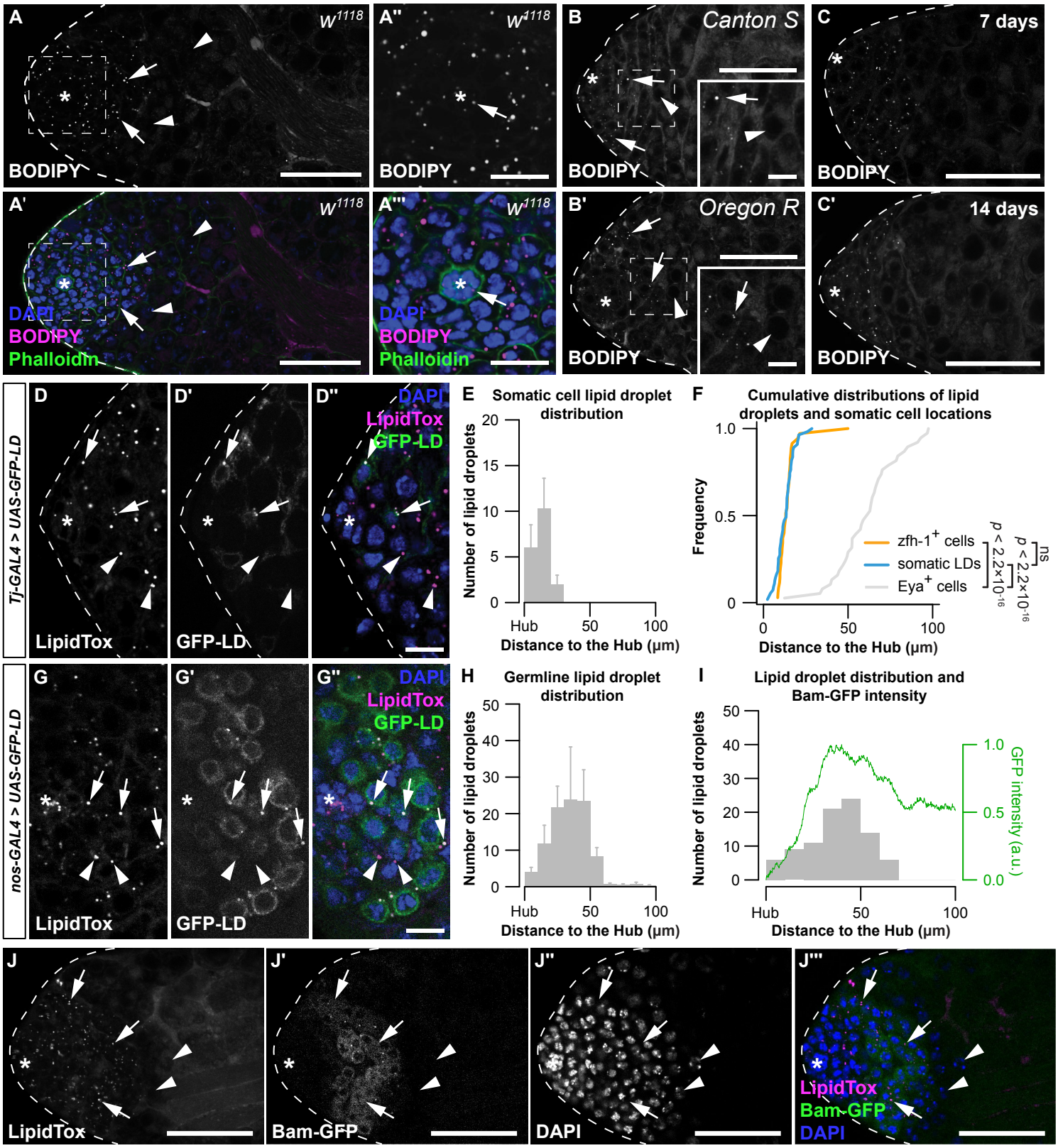

Figure 2 – *brummer* regulates testis lipid droplets in a cell-autonomous manner.

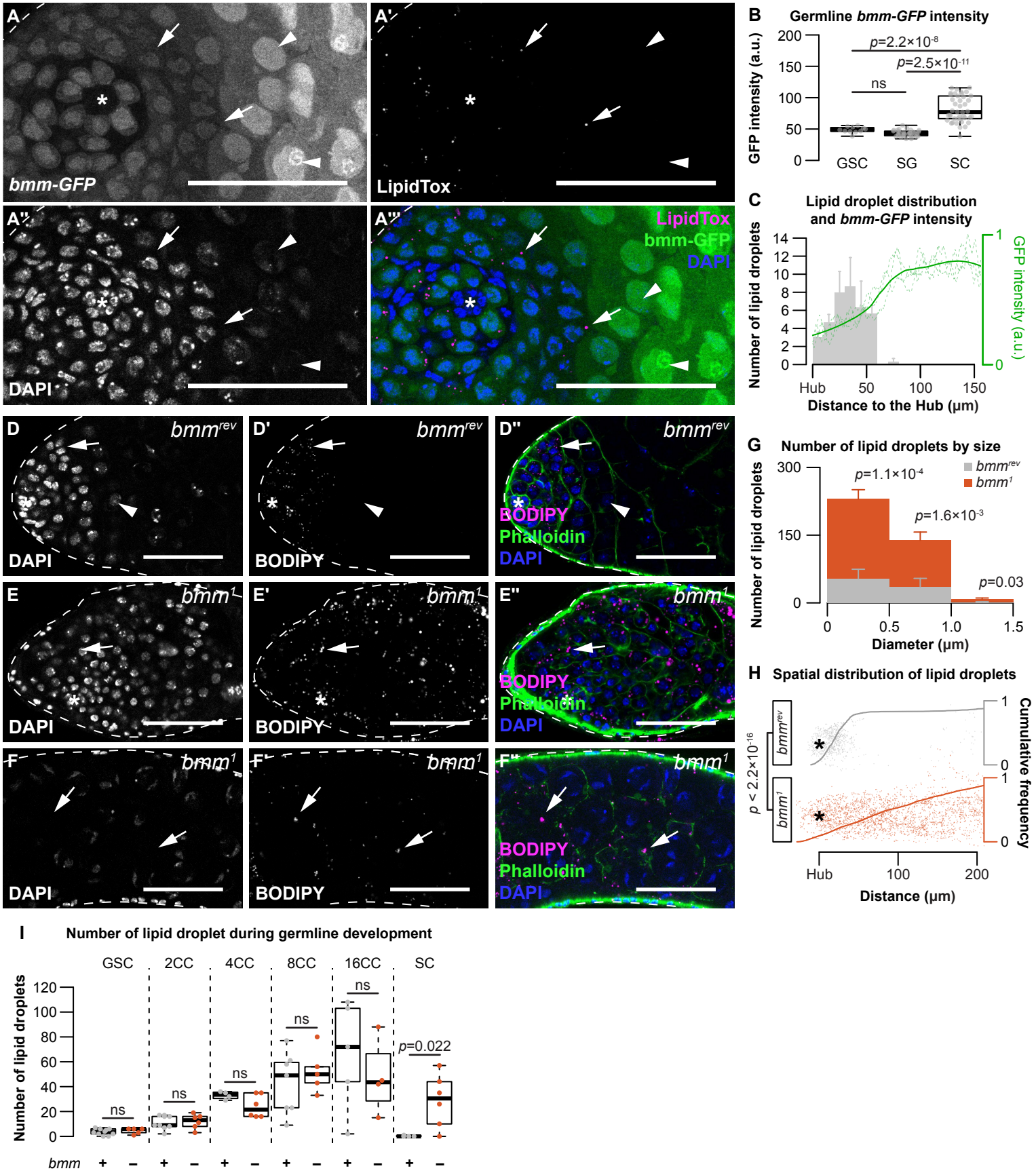

Figure 3 – A cell-autonomous role of *brummer* in regulating spermatogenesis.

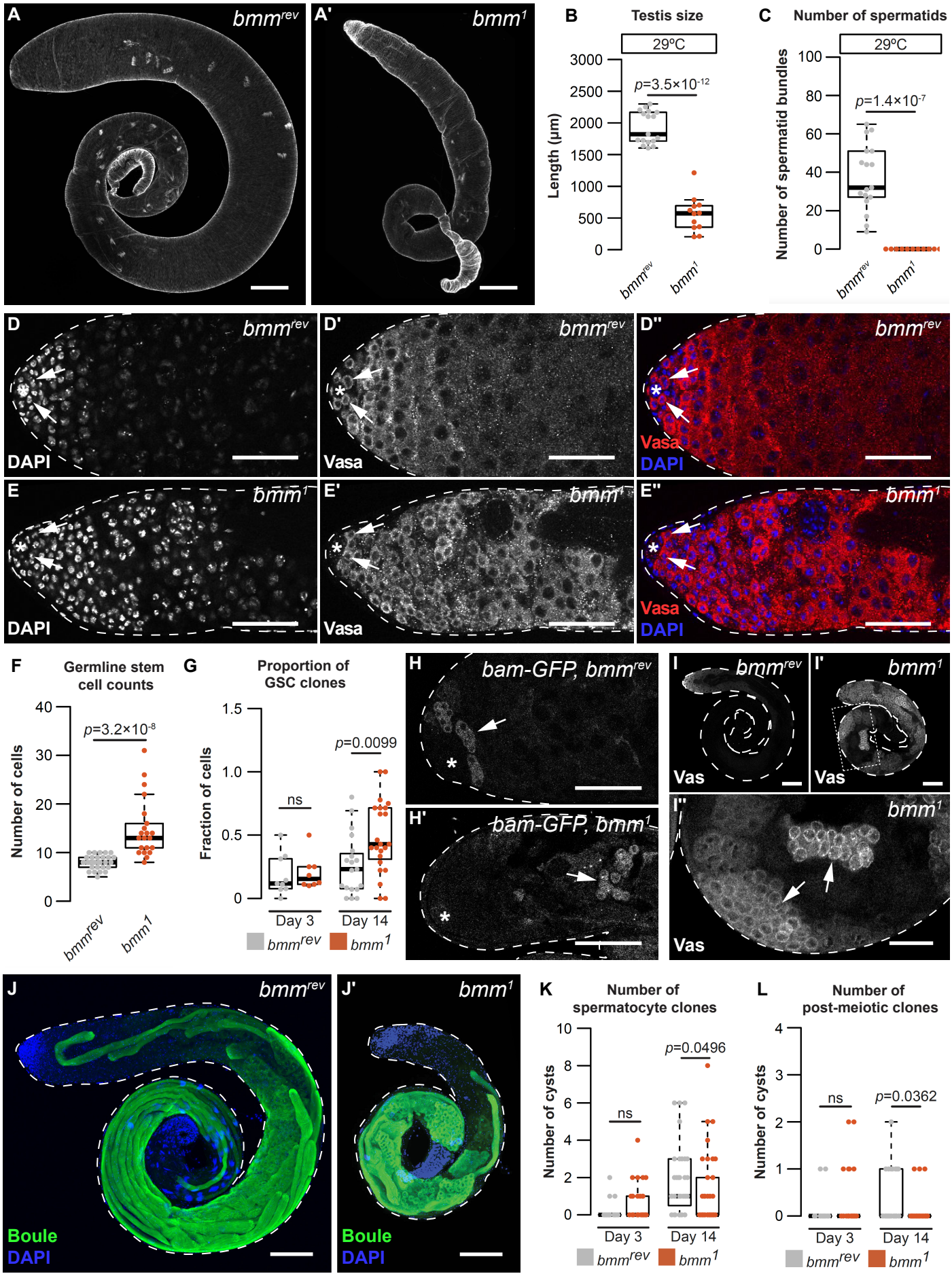

Figure 4 – Loss of *brummer* disrupts triglyceride homeostasis and leads to spermatogenic defects.

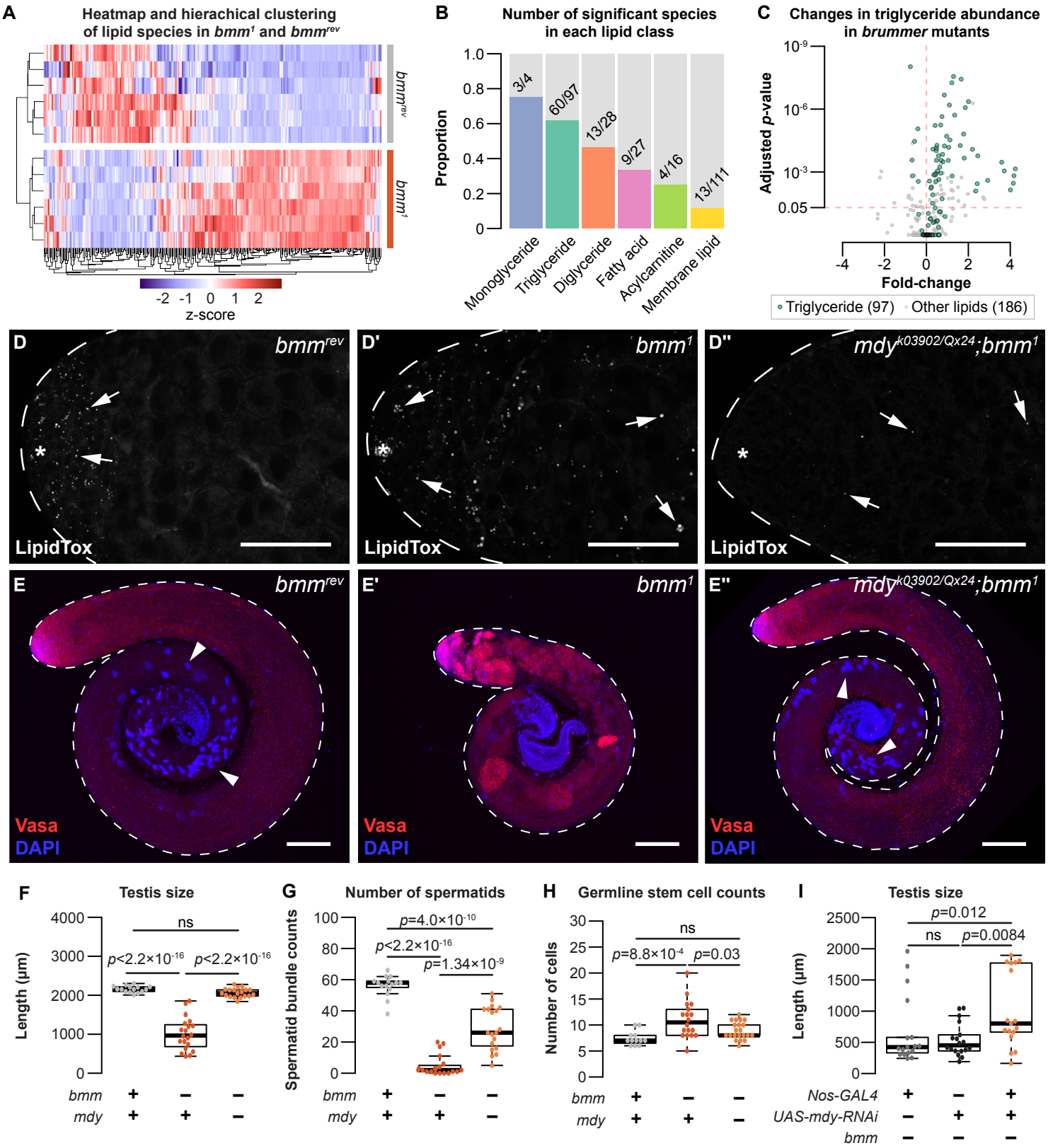

Supplemental Figure 1 – Cholesterol is absent from testis lipid droplets.

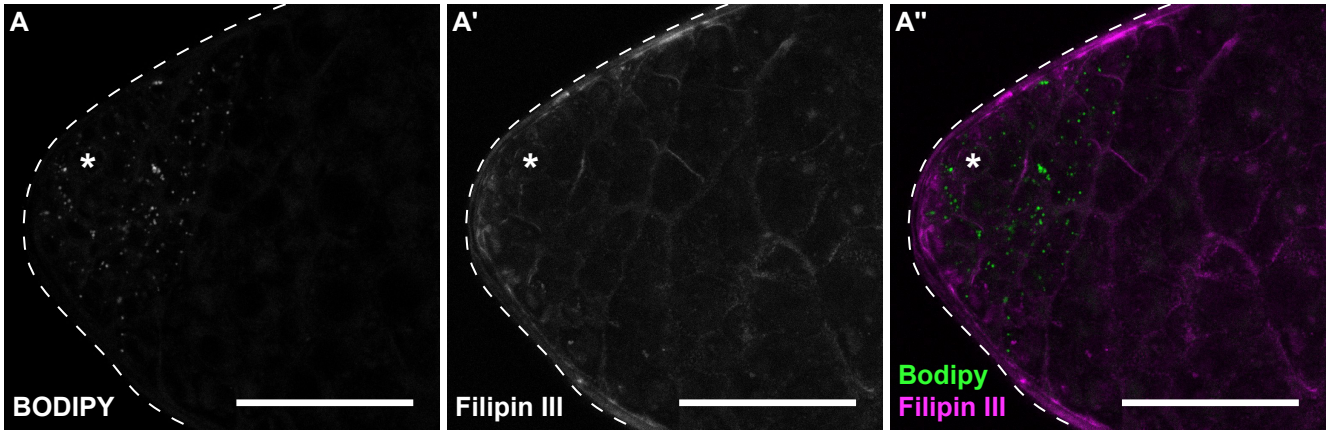

Supplemental Figure 2 – *brummer* regulates testis lipid droplets in a cell-autonomous manner.

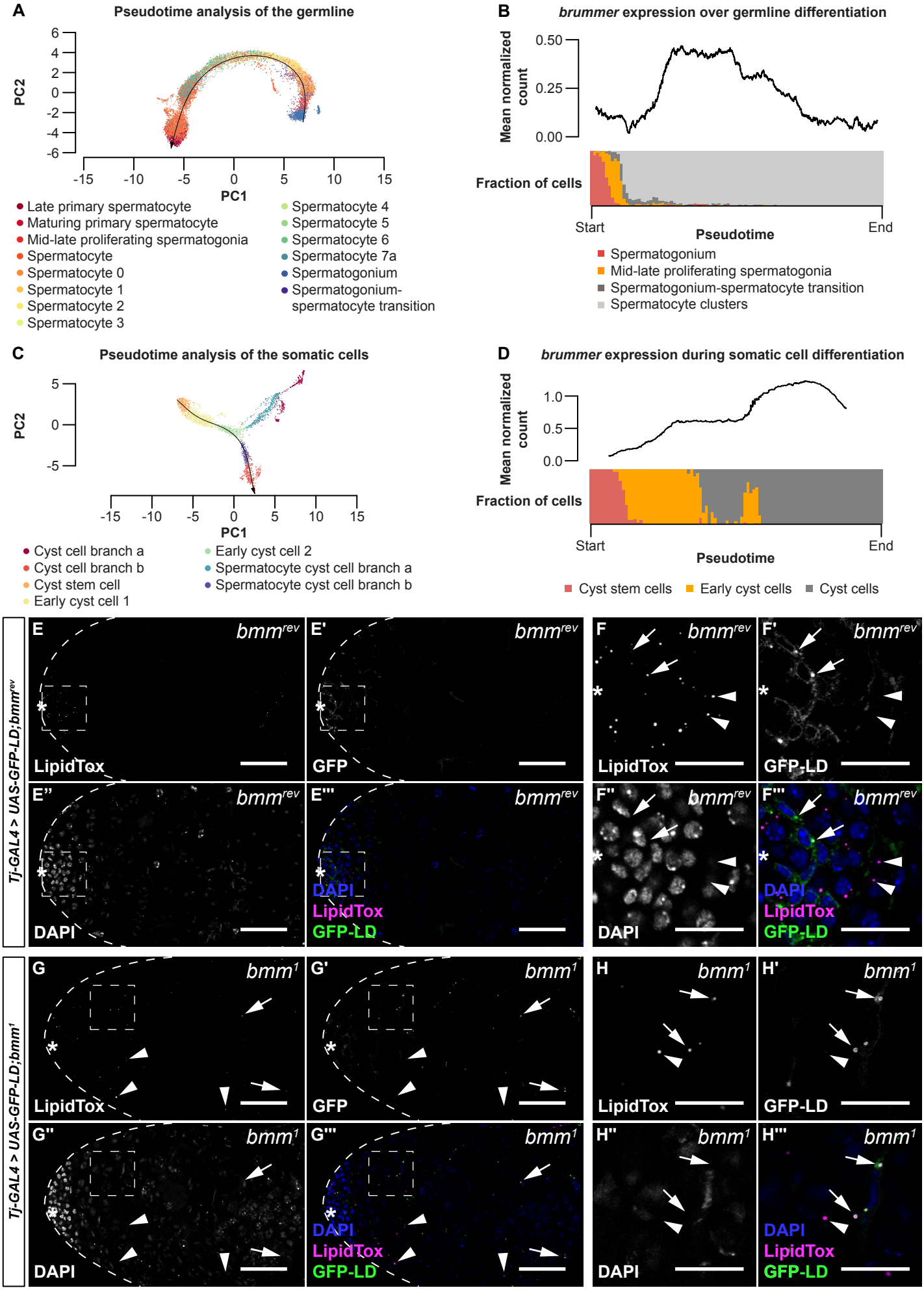

Supplemental Figure 3 – Additional characterization of testis development and spermatogenesis in animals lacking *brummer*.

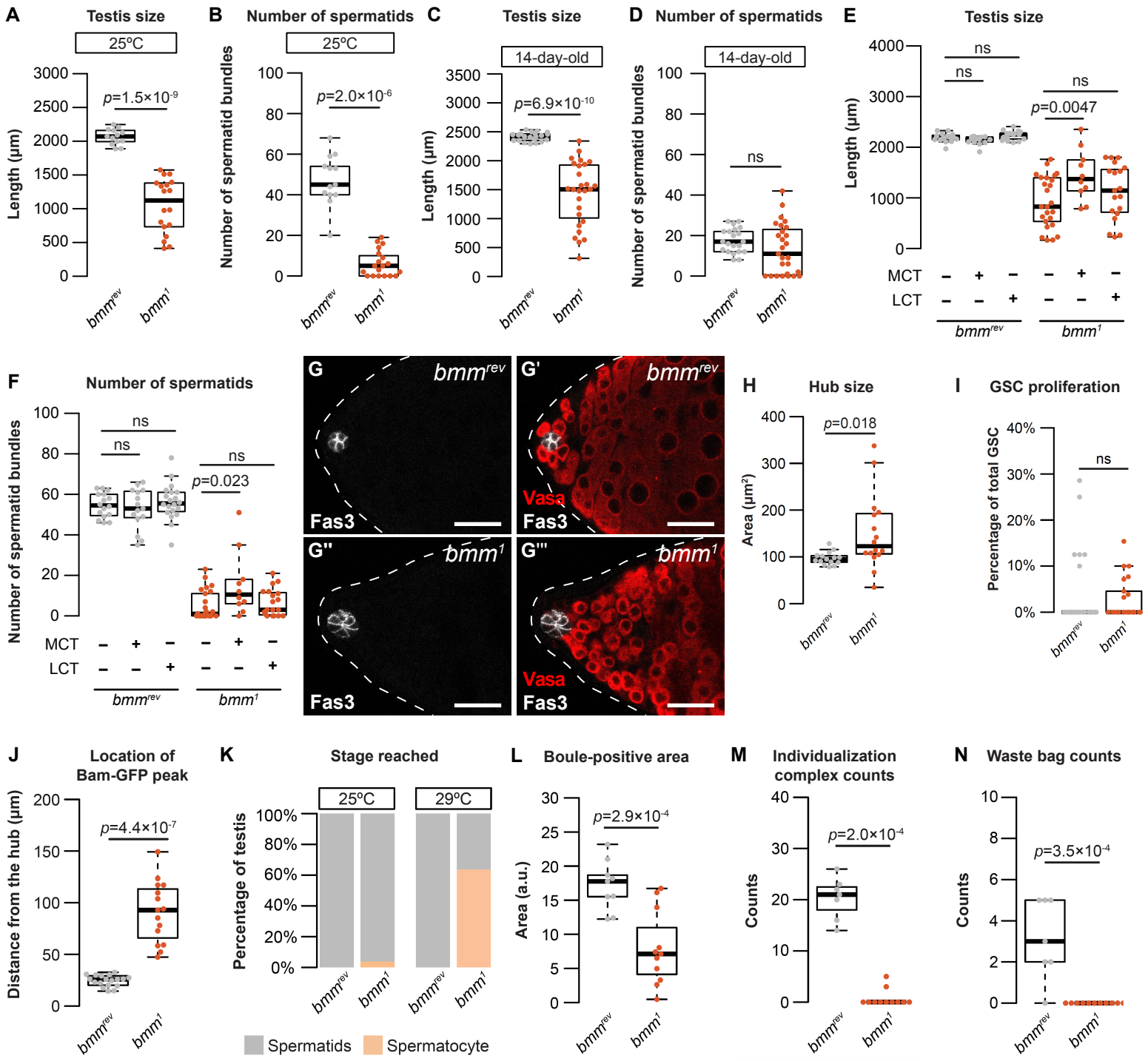
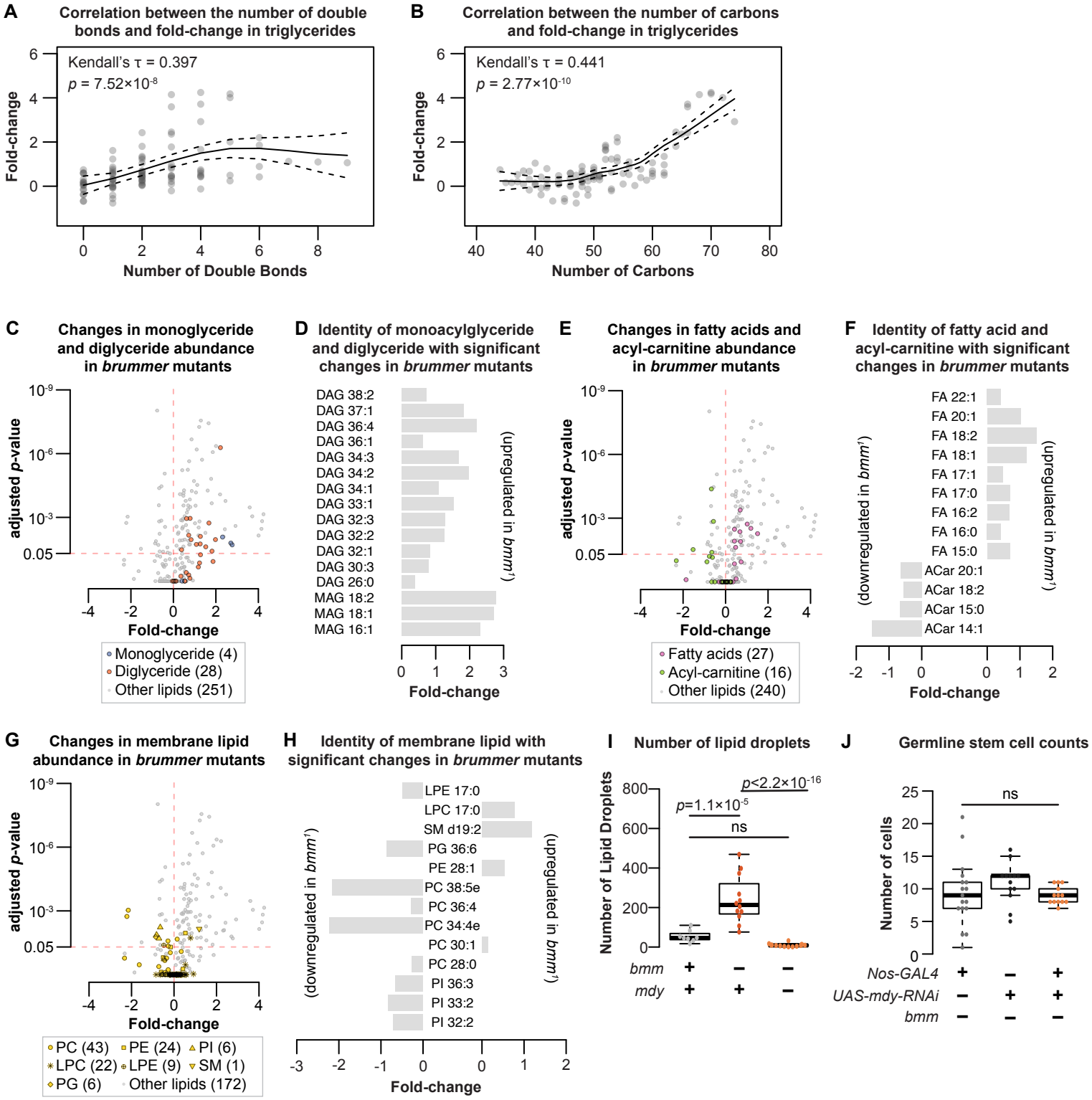
Supplemental Figure 4 – Lipidomic analysis of animals lacking *brummer*.